



## AUTOIMMUNITY

# UNC93B1 variants underlie TLR7-dependent autoimmunity

Christine Wolf<sup>1</sup>, Ee Lyn Lim<sup>2</sup>, Mohammad Mokhtari<sup>3</sup>, Barbara Kind<sup>1</sup>, Alexandru Odainic<sup>4,5</sup>, Eusebia Lara-Villacanas<sup>6</sup>, Sarah Koss<sup>1</sup>, Simon Mages<sup>3</sup>, Katharina Menzel<sup>1</sup>, Kerstin Engel<sup>1</sup>, Gregor Dückers<sup>7</sup>, Benedikt Bernbeck<sup>6</sup>, Dominik T. Schneider<sup>6</sup>, Kathrin Siepermann<sup>7</sup>, Tim Niehues<sup>7</sup>, Carl Christoph Goetzke<sup>8,9,10</sup>, Pawel Durek<sup>9</sup>, Kirsten Minden<sup>8,9</sup>, Thomas Dörner<sup>9,11</sup>, Anna Stittrich<sup>12</sup>, Franziska Szelinski<sup>9,11</sup>, Gabriela Maria Guerra<sup>9</sup>, Mona Massoud<sup>9</sup>, Markus Bieringer<sup>13</sup>, Carina C. de Oliveira Mann<sup>14</sup>, Eduardo Beltrán<sup>15</sup>, Tilmann Kallinich<sup>8,9,10</sup>, Mir-Farzin Mashreghi<sup>9</sup>, Susanne V. Schmidt<sup>4</sup>, Eicke Latz<sup>4,16</sup>, Johanna Klughammer<sup>3</sup>, Olivia Majer<sup>2</sup>, Min Ae Lee-Kirsch<sup>1,17\*</sup>

Copyright © 2024 the Authors, some rights reserved; exclusive licensee American Association for the Advancement of Science. No claim to original U.S. Government Works

UNC93B1 is critical for trafficking and function of nucleic acid-sensing Toll-like receptors (TLR) TLR3, TLR7, TLR8, and TLR9, which are essential for antiviral immunity. Overactive TLR7 signaling induced by recognition of self-nucleic acids has been implicated in systemic lupus erythematosus (SLE). Here, we report UNC93B1 variants (E92G, R336L) in four patients with early-onset SLE. Patient cells or mouse macrophages carrying the UNC93B1 variants produced high amounts of TNF- $\alpha$  and IL-6 and upon stimulation with TLR7/TLR8 agonist, but not with TLR3 or TLR9 agonists. E92G causes UNC93B1 protein instability and reduced interaction with TLR7, leading to selective TLR7 hyperactivation with constitutive type I IFN signaling. Thus, UNC93B1 regulates TLR subtype-specific mechanisms of ligand recognition. Our findings establish a pivotal role of UNC93B1 in TLR7-dependent autoimmunity and highlight the therapeutic potential of targeting TLR7 in SLE.

## INTRODUCTION

Endosomal Toll-like receptors (TLRs) play a fundamental role in detecting pathogen-derived nucleic acids. Single-stranded RNA (ssRNA) is recognized by TLR7 and TLR8, double-stranded RNA (dsRNA) by TLR3, and ssDNA by TLR9 (1, 2). TLRs consist of a single transmembrane  $\alpha$ -helix with a luminal ectodomain containing a leucine-rich repeat (LRR-CT motif) and a cytoplasmic Toll/interleukin-1 receptor (TIR) domain (3). Upon ligand recognition through the LRR-CT motif, the TIR domains of the TLR homodimer assemble to form signaling complexes. Activation of TLR7, TLR8, and TLR9 initiates recruitment of the adaptor protein myeloid differentiation primary-response protein 88 (MyD88), while engagement of TLR3 induces recruitment of

TIR domain-containing adaptor protein inducing IFN- $\beta$  (TRIF) (1, 2). Both pathways lead to activation of interferon-regulatory factor (IRF) 7, IRF3 and nuclear factor- $\kappa$ B (NF- $\kappa$ B), resulting in induction of type I IFN and pro-inflammatory cytokines that mobilize host immune responses (1, 2).

The multipass transmembrane chaperone UNC93B1 is required for the trafficking of TLRs from the endoplasmic reticulum to the endosome and acts as a scaffold for proper configuration of the TLR dimer within the endosomal membrane, which is critical for TLR signaling (4–7). The essential role of UNC93B1 for nucleic acid-sensing TLR function was unraveled by studying 3d mice, which harbor a mutation in *Unc93b1* (H412R) that abrogates endosomal TLR signaling (8). Consistently, patients with loss-of-function mutations in *UNC93B1* are highly susceptible to herpes encephalitis due to absent endosomal TLR function (9). In addition to its trafficking role, UNC93B1 has also been shown to be important for TLR5 function on the cell surface (10), maintenance of endosomal TLR expression and protein stability (5, 6), and termination of TLR7 signaling via syntenin-1 (11).

Abnormally enhanced TLR7 signaling induced by aberrant immune recognition of self-nucleic acids has been shown to cause systemic autoimmunity in mice and humans (11–17). Notably, two distinct *Unc93b1* mutations (D34A, PKP530–532) that lead to TLR7 hyperactivation cause lupus-like features in mice (11, 15), suggesting a role of UNC93B1 in selectively restraining aberrant TLR7 activation. Structural data on the UNC93B1/TLR7 complex suggests that UNC93B1 prevents TLR7 activation by inhibiting ligand-induced dimerization (7, 18). However, the mechanisms that restrict premature or accidental activation of TLR7 remain unclear. Here, we describe missense *UNC93B1* variants that underlie uncontrolled TLR7 hyperactivation in patients with early-onset systemic lupus erythematosus (SLE).

<sup>1</sup>Department of Pediatrics, Medizinische Fakultät Carl Gustav Carus, Technische Universität Dresden; Dresden, 01307, Germany. <sup>2</sup>Max Planck Institute for Infection Biology; Berlin, 10117, Germany. <sup>3</sup>Gene Center, Systems Immunology, Ludwig-Maximilians-Universität München; Munich, 81377, Germany. <sup>4</sup>Institute of Innate Immunity, University of Bonn; Bonn, 53127, Germany. <sup>5</sup>Department of Microbiology and Immunology, The Peter Doherty Institute for Infection & Immunity, University of Melbourne; Melbourne, VIC 3010, Australia. <sup>6</sup>Department of Pediatrics, Klinikum Dortmund, University Witten/Herdecke; Dortmund, 44145, Germany. <sup>7</sup>Department of Pediatrics, Helios Klinik Krefeld; Krefeld, 47805, Germany. <sup>8</sup>Department of Pediatric Respiratory Medicine, Immunology and Critical Care Medicine, Charité-Universitätsmedizin Berlin; Berlin, 10117, Germany. <sup>9</sup>Deutsches Rheuma-Forschungszentrum (DRFZ), an Institute of the Leibniz Association; Berlin, 10117, Germany. <sup>10</sup>Berlin Institute of Health at Charité-Universitätsmedizin Berlin; Berlin, 10178, Germany. <sup>11</sup>Department of Medicine, Rheumatology and Clinical Immunology, Charité-Universitätsmedizin Berlin; Berlin, 10117, Germany. <sup>12</sup>Labor Berlin Charité-Vivantes GmbH, Department of Human Genetics; Berlin, 13353, Germany. <sup>13</sup>Department of Cardiology and Nephrology, HELIOS Klinikum Berlin-Buch; Berlin, 13125, Germany. <sup>14</sup>Institute of Virology, Technical University of Munich; Munich, 81675, Germany. <sup>15</sup>Institute for Clinical Neuroimmunology, BioMedizinisches Zentrum, Ludwig-Maximilians-Universität München; Munich, 82152, Germany. <sup>16</sup>German Center for Neurodegenerative Diseases (DZNE); Bonn, 53175, Germany. <sup>17</sup>University Center for Rare Diseases, Medizinische Fakultät Carl Gustav Carus, Technische Universität Dresden; Dresden, 01307, Germany.

\*Corresponding author. Email: minae.lee-kirsch@uniklinikum-dresden.de

**RESULTS****UNC93B1 variants in patients with early-onset systemic lupus erythematosus**

We investigated two siblings from a consanguineous family of Madeiran ancestry (family A, Fig. 1A). Patient 1 developed first symptoms of SLE at 4 months of age, including refractory autoimmune thrombocytopenia, autoimmune anemia, and erythematous rash, followed by hepatosplenomegaly, glomerulonephritis, arthritis, and panniculitis over the following 6 years; patient 2 presented with anemia, malar rash, renal disease, vasculitis, and seizures beginning at 2 years of age (table, S1 and S2). Both children exhibited multiple autoantibodies, including antinuclear antibodies (ANA) and anti-dsDNA, as well as strongly elevated IFN scores in peripheral blood mononuclear cells (PBMC), as shown by increased expression of IFN-stimulated genes (Fig. 1B, table, S1 and S2). Levels of pro-inflammatory cytokines, IL-6, IL-8, and TNF- $\alpha$ , in serum and in medium of cultured lymphoblastoid cells (LCLs) were markedly increased in both patients (Fig. 1, C and D), compared to wild type controls and a previously reported UNC93B1-deficient control (9). Whole-exome sequencing revealed a homozygous variant in *UNC93B1* (c.275A > G, p.E92G; NM\_030930.4) in both children, affecting a highly conserved amino acid residue located within the first luminal loop (Fig. 1, E to G). Both healthy parents were heterozygous carriers of the E92G variant which was reported once in the gnomAD database and predicted to impair function (Fig. 1E, table S3).

The second family (family B) is of European German ancestry (Fig. 1A). The son, patient 3, presented first signs of SLE at 18 months of age, including dermatitis, positive ANAs and hypocomplementemia. At 16 years, he developed hepatomegaly, progressive generalized lymphadenopathy, and arthralgia. At 19 years, he was noted to have proteinuria, hyperglobulinemia, anti- $\beta$ 2-glycoprotein, and anti-dsDNA-antibodies (table, S1 and S2). His father, patient 4, presented first symptoms at 5 years of age, including malar rash, photosensitivity, arthralgia, and positive ANAs. At 30 years, he developed lupus nephritis (Fig. 1A, table, S1 and S2). Similar to the patients of family A, both affected members of family B exhibited strong IFN signatures and elevated pro-inflammatory serum cytokines (Fig. 1B, fig. S1). Whole-exome sequencing led to the identification of a heterozygous previously undescribed *UNC93B1* variant (c.1007G > T, p.R336L), which is highly conserved and predicted to be damaging (Fig. 1, E to G, table S3). In both families, no other mutations, including variants of unknown significance, or copy number variants in genes previously implicated in autoimmune lymphoproliferative syndrome (ALPS) or other monogenic forms of lupus were found.

**SLE-associated transcriptional signatures in patient cells**

To study the transcriptional changes related to *UNC93B1*<sup>E92G</sup> in a cell type-resolved manner, we performed single-cell RNA (scRNA) sequencing in PBMCs from patient 1 and a sex- and age-matched healthy control. A total of 3354 and 5906 cells for patient 1 and control, respectively, were retained for analysis after filtering out doublets and low quality cells. We annotated nine distinct cell types covering all expected cell types (Fig. 2, A to C). Consistent with migration of plasmacytoid dendritic cells (pDCs) into tissues upon activation by self-nucleic acid-containing immune complexes (19, 20), pDCs were underrepresented in the patient sample (Fig. 2B). In line with clinical data (table S4) and previous single cell data from SLE patients (21), there was a reduction of CD4<sup>+</sup> helper T cells and an expansion of cytotoxic CD8<sup>+</sup> T cells (Fig. 2B). Likewise, CD8<sup>+</sup> T cells exhibited a cytotoxic signature (*PRF1*, *GZMH*, *GZMB*) and an exhaustion

signature (*PDCD1*, *CTLA4*, *LAG3*, *CD160*, *TIGIT*, *HAVCR2*, *CD244*), in addition to a generally increased IFN signature (Fig. 2, D and E). In fact, patient cells exhibited elevated expression of IFN-stimulated genes (ISGs) across all cell types, but most prominently in monocytes and dendritic cells (Fig. 2D). Differential gene expression analysis and gene ontology (GO) term enrichment analysis revealed cell type-specific transcriptional responses in patient cells compared to the control, including activation of B cells in terms of cell cycle regulation (GO:0051726), up-regulation of IL-12 signaling (GO:0071349) in CD4<sup>+</sup> T cells as well as induction of IFN- $\gamma$  (GO:0032729) and TNF- $\alpha$  (GO:0010803) in CD8<sup>+</sup> T cells, indicative of T cell activation (Fig. 2F). Similar to children with complex SLE (19), CD8<sup>+</sup> T cells, NK cells, and CD16<sup>+</sup> monocytes exhibited a distinct IL-1 $\beta$  signature (GO:0050718), while CD14<sup>+</sup> and CD16<sup>+</sup> monocytes featured a response to LPS (GO:0032496), with upregulation of NF- $\kappa$ B in CD16<sup>+</sup> monocytes (GO:0051092) (Fig. 2F).

To assess the general validity of the transcriptional cellular phenotypes observed in patient 1 and to gain further insight into rare cell subtypes, we assessed FACS-sorted PBMCs (enriched for T cells, B cells, monocytes and pDCs) of patient 3 who carries the *UNC93B1*<sup>R336L</sup> mutation (fig. S2, A to D). These orthogonal data largely confirmed the cell type-specific transcriptional phenotypes described for patient 1, in particular the IFN signature and cytotoxic phenotype in CD8<sup>+</sup> T cells (fig. S2, B and C). Furthermore, peripheral B cells from patient 3 showed an increase in CD27<sup>high</sup> CD38<sup>high</sup> plasmablasts compared to healthy controls (fig. S3), consistent with enhanced B cell hyperactivity, as well as an increase in double-negative CD27<sup>-</sup> IgD<sup>-</sup> B cells (fig. S3), a distinct memory B cell subset commonly expanded in SLE (16, 22). Collectively, these findings indicate that cell type-specific transcriptional signatures and B cell phenotypes of the patients carrying *UNC93B1* mutations are highly similar to those observed in complex SLE.

**Constitutive activation of ssRNA-sensing TLRs in patient cells**

Given the essential role of *UNC93B1* for endosomal TLR function and the observed chronic type I IFN activation in the patients, we hypothesized that the identified *UNC93B1* mutations might underlie hyperactivation of TLR-dependent nucleic acid-sensing pathways. To investigate the signaling properties of *UNC93B1*-dependent TLRs in patient cells, we measured cytokine responses using specific agonists. Following stimulation with R848, an imidazoquinoline compound with TLR7/TLR8 agonist activity, patient PBMCs (P1, P2) produced markedly higher levels of TNF- $\alpha$  compared to wild type controls (Fig. 3A). In contrast, IP-10 secretion by PBMCs in response to the TLR9 agonist ODN2006 and IL-8 secretion by primary fibroblasts in response to the TLR3 agonist polyinosinic-polycytidylic acid (poly(I:C)) did not differ between patients and controls (Fig. 3A). Likewise, patient LCLs also produced much higher amounts of IL-6 and TNF- $\alpha$ , both at basal level and in response to R848, than LCLs from wild type controls or a patient carrying a loss-of-function *UNC93B1* mutation (9), while patient LCLs showed normal responses to ODN2006 (Fig. 1D, fig. S4, A and B). Stimulation of *UNC93B1*-independent TLR2 (Pam2CSK4) in LCLs or TLR4 (lipopolysaccharide; LPS) in fibroblasts did not reveal any differences between patients and controls (fig. S4, C and D). To further assess TLR7-specific hyperactivation, we stimulated whole blood of patients carrying either the *UNC93B1*<sup>E92G</sup> or the *UNC93B1*<sup>R336L</sup> mutation with selective agonists. Treatment with the TLR7 agonist R837 resulted in

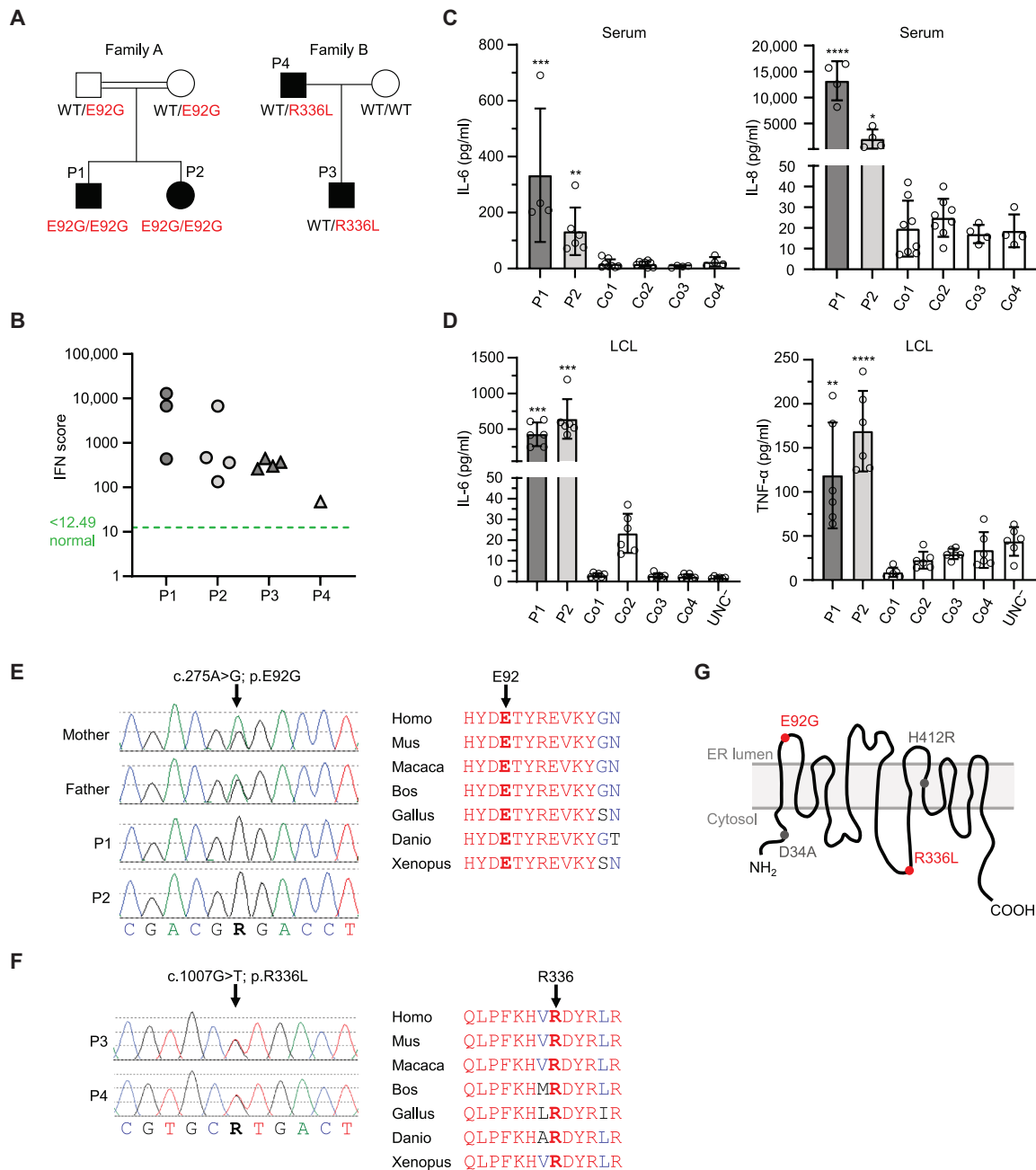


**Fig.1. Identification of *UNC93B1* mutations in two families with early-onset SLE. (A)** Pedigrees of families with *UNC93B1* mutations. **(B)** IFN scores in PBMCs of patients (P1, P2, P3 and P4) based on qRT-PCR. An IFN score of 12.49 (dashed green line) indicates the median IFN score of 10 healthy controls +2 SD. **(C)** Levels of pro-inflammatory cytokines (IL-6, IL-8) in patient sera, collected at different time points, compared to four healthy controls (Co1-Co4). \*,  $P < 0.05$ ; \*\*,  $P < 0.01$ \*\*\*;  $P < 0.001$ ; \*\*\*\*;  $P < 0.0001$  vs. mean of wild type controls, Kruskal-Wallis test (Dunn's multiple comparisons test) for IL-6; One-way ANOVA (Dunn's multiple comparisons test) for IL-8. **(D)** Levels of IL-6 and TNF- $\alpha$  secreted by LCLs from two patients (P1, P2), four wild type controls (Co1-Co4) and an *UNC93B1*-deficient individual (UNC). Mean  $\pm$  SD of at least four independent experiments. \*,  $P < 0.05$ ; \*\*\*\*;  $P < 0.0001$  vs. mean of wild type controls, Kruskal-Wallis test (Dunn's multiple comparisons test). **(E and F)** Electropherograms showing *UNC93B1* mutations and multiple sequence alignment showing high conservation of E92 (E) and R336 (F) of the *UNC93B1* protein. **(G)** Schematic of *UNC93B1* topology depicting human mutations (E92G, R336L) and mouse mutations D34A (gain-of-function) and H412R (loss-of-function).

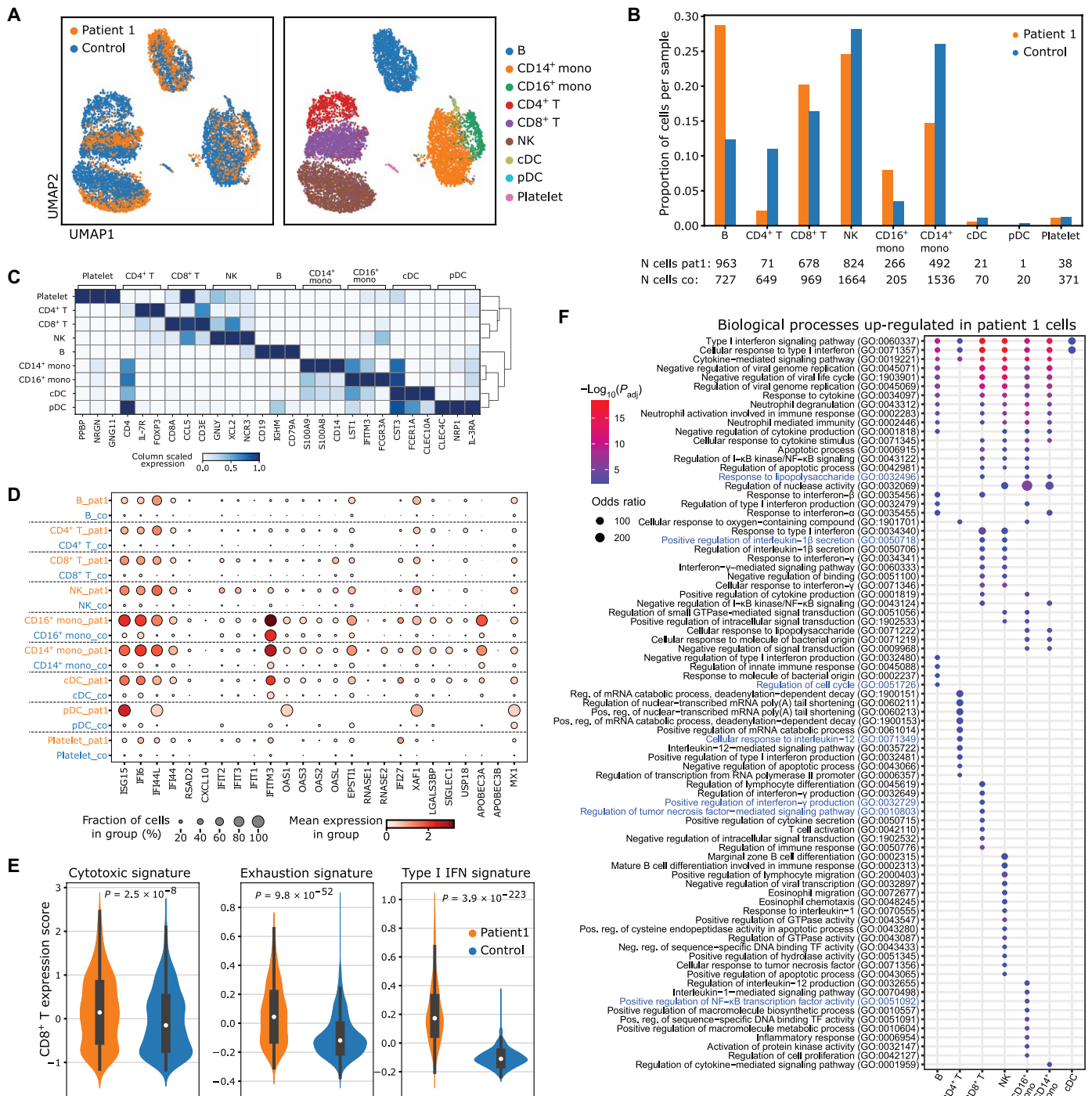


**Fig. 2. Single-cell RNA sequencing of PBMCs of patient 1 and control.** (A) Integrated uniform manifold approximation and projection (UMAP) of data from patient 1 and one age- and sex-matched control, assigned to 9 cell subtypes: B cells (B); monocytes (mono: CD16<sup>+</sup> and CD14<sup>+</sup>); T cells (T: CD8<sup>+</sup> and CD4<sup>+</sup>); natural killer cells (NK); conventional dendritic cells (cDC); plasmacytoid dendritic cells (pDC); platelets. (B) Bar graph displaying the individual cell type proportions in patient 1 and control, with corresponding absolute cell numbers. (C) Heatmap displaying relative marker gene expression across cell types. (D) Dot plot showing cell type-specific ISG expression. (E) Violin plots depicting cytotoxic, exhaustion, and IFN signatures in CD8<sup>+</sup> T cells, comparing patient and control cells. Two-sided Wilcoxon Rank Sum Test. (F) Dot-plot showing the GO terms that are enriched in genes, overexpressed in the patient cells compared to control cells for each of the indicated cell types. Two-sided Fisher's exact test corrected for multiple testing (FDR).

Downloaded from https://www.science.org at Max Planck Society on February 19, 2024



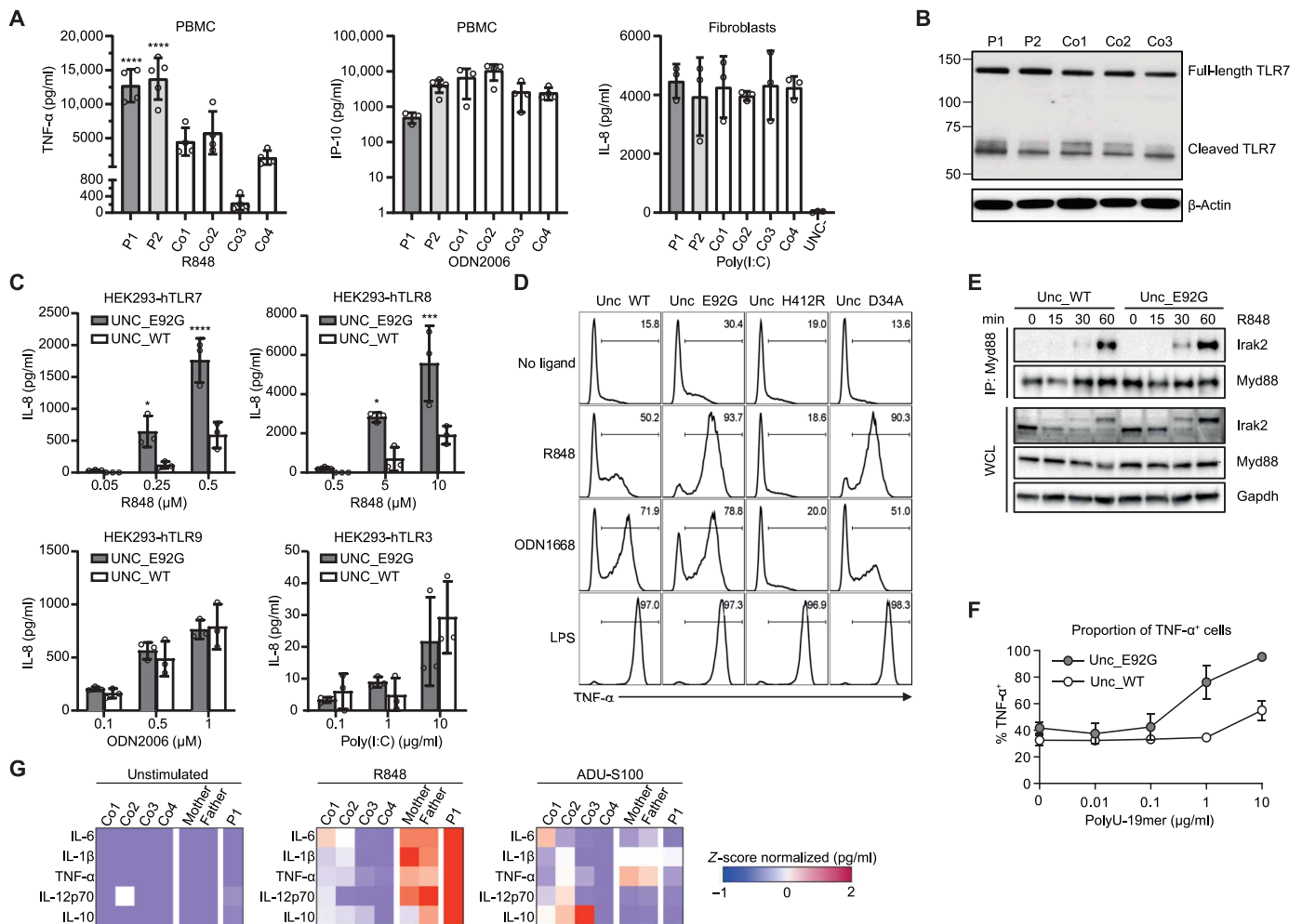


**Fig. 3. Functional consequences of the E92G UNC93B1 mutation on TLR signaling.** (A) Secretion of TNF- $\alpha$  and IP-10 by PBMCs following stimulation with the TLR7/8 agonist R848 (1  $\mu$ g/ml) or the TLR9 agonist ODN2006 (0.5  $\mu$ M), and secretion of IL-8 by fibroblasts following stimulation with the TLR3 agonist poly(I:C) (10  $\mu$ g/ml). Patients (P1, P2), controls (Co1-Co4), UNC93B1-deficient control (UNC-). Mean  $\pm$  SD of at least three technical replicates. One-way ANOVA (Dunnett's multiple comparisons test). \*\*\*\*,  $P < 0.0001$  vs. controls. \*\*\*\*,  $P < 0.0001$  vs. controls. (B) Expression of full-length and cleaved TLR7 in LCLs.  $\beta$ -actin was probed as loading control. (C) Secretion of IL-8 by TLR-expressing HEK293 cells transduced with mutant (UNC\_E92G) or wild type (UNC\_WT) UNC93B1 using the indicated agonists. Mean  $\pm$  SD of three technical replicates. Two-way ANOVA (Bonferroni's multiple comparisons test). \*,  $P < 0.05$ ; \*\*\*,  $P < 0.001$ ; \*\*\*\*,  $P < 0.0001$  vs. UNC\_WT. (D) Production of TNF- $\alpha$  in *Unc93b1*<sup>-/-</sup> mouse RAW264.7 macrophages re-constituted with *Unc93b1* variants stimulated with the indicated TLR agonists. (E) Myddosome formation assayed by co-immunoprecipitation of whole cell lysates (WCL) from *Unc93b1*-reconstituted *Unc93b1*<sup>-/-</sup> RAW264.7 cells using anti-Myd88 antibody, followed by Western blot analysis using anti-Irk2 antibody. Gapdh was immune-stained as loading control. (F) Proportion of TNF- $\alpha$ -positive cells in *Unc93b1*-reconstituted *Unc93b1*<sup>-/-</sup> RAW264.7 cells after stimulation with polyU-ssRNA. Mean  $\pm$  SD of four technical replicates. Data are representative of at least three (A to C) or two (D to F) independent experiments. (G) Heatmap of inflammatory cytokines after stimulation of whole blood from four healthy controls (Co1-Co4), P1 and his parents (mother, father) with R848 and ADU-S100.

a strong IL-6 production by patient cells compared to wild type controls (fig. S5), corroborating TLR7 hyperactivation. While patient cells also displayed hyperresponsiveness to the TLR8 agonist TL8-506, their cytokine response to the TLR9 agonist ODN2216 did not differ from wild type controls (fig. S5).

Similar to R848, endosomal delivery of RNA40, a well-established 20-mer ssRNA ligand specific for TLR7/TLR8 (23), resulted in a much higher TNF- $\alpha$  secretion in patient PBMCs than in controls (fig. S6). The presence of hydroxychloroquine (HCQ), an antimalarial drug that impedes nucleic acid recognition by endosomal TLRs (24), reduced signaling in both wild type and mutant cells (fig. S6), consistent with hyperactivation of TLR7/8 in endosomes. Moreover,

we observed similar ratios of full-length and cleaved TLR7 in LCLs from both patients carrying the *UNC93B1*<sup>E92G</sup> mutation and wild type controls (Fig. 3B). Since cleavage of full-length TLR7 occurs within the acid environment of the endosome, this further demonstrates that TLR trafficking as such is not affected by the *UNC93B1*<sup>E92G</sup> mutation.

IFN- $\alpha$  up-regulates TLR7 expression in B cells, promotes cell death and release of self-nucleic acids, and primes pDCs to respond more effectively to immune complexes (25, 26). Accordingly, TLR7 expression in patient 1 was slightly up-regulated only in B cells, but not in any of the other assessed PBMC cell types, while in patient 3, TLR7 was slightly up-regulated in B cells, monocytes, and pDCs, but

not correlated with *IFNA1* or *ISG15* gene expression (fig. S7, A to D). We also confirmed that pDCs, the main IFN- $\alpha$ -producing cells able to secrete up to 1000 times more type I IFNs than any other white blood cell, did not significantly express TLR8 (27, 28) in either patient (fig. S7, A and C). Together, these findings suggest that type I IFN activation in patients carrying the *UNC93B1*<sup>E92G</sup> or *UNC93B1*<sup>R336L</sup> mutation is likely caused by hyperactivation of the TLR7 signaling pathway that is not due to an increased expression of *TLR7*.

### Recapitulation of TLR7 hyperactivation in HEK293 cells and mouse macrophages

To further exclude that hyperactivation of ssRNA-sensing TLRs observed in *UNC93B1*<sup>E92G</sup> patient cells was caused by up-regulation of TLR7/TLR8 due to systemic type I IFN activation, we studied HEK293 cells with stable expression of endosomal TLRs. To facilitate endosomal targeting and signaling of TLRs (4), we co-expressed *UNC93B1*. TLR-expressing HEK293 cells were transfected with citrine-tagged *UNC93B1* variants and sorted by flow cytometry to ensure equal expression (fig. S8). In HEK293 cells expressing either TLR7 or TLR8 (HEK293-hTLR7, HEK293-hTLR8), stimulation with R848 markedly increased IL-8 secretion in the presence of the E92G mutant compared to cells expressing wild type *UNC93B1* (Fig. 3C). Similarly, endosomal delivery of RNA40 to HEK293-hTLR7 led to higher IL-8 production in the presence of mutant *UNC93B1*, compared to wild type *UNC93B1*, which was reduced by HCQ (fig. S9A). In contrast, stimulation of HEK293-hTLR9 or HEK293-hTLR3 with their cognate ligands, ODN2006 or poly(I:C), respectively, or endosomal delivery of ODN2006 to HEK293-hTLR9 led to comparable IL-8 production, irrespective of the presence of mutant or wild type *UNC93B1* (Fig. 3C, fig. S9B).

We next investigated TLR signaling in transgenic RAW 264.7 *Unc93b1*<sup>-/-</sup> murine macrophages stably expressing equal levels of mouse *Unc93b1* variants (E92G, D34A, H412R; fig. S10A). No differences in Tlr7 expression was observed in *Unc93b1*<sup>-/-</sup> murine macrophages reconstituted with *Unc93b1* variants (fig. S10A). In response to R848 stimulation, TNF- $\alpha$  production in cells carrying the E92G mutation was significantly stronger compared to cells expressing wild type *Unc93b1* (Fig. 3D). This was accompanied by enhanced Myddosome formation, the most proximal signaling step downstream of TLR7 activation, as shown by recruitment and post-translational modification of Irak2 (Fig. 3E). In contrast, no differences were observed when cells were stimulated with the TLR9 ligand ODN1668 (Fig. 3D), confirming a TLR7-specific activating effect conferred by the *Unc93b1*<sup>E92G</sup> variant. As expected, in presence of the loss-of-function mutant *Unc93b1*<sup>H412R</sup>, which abrogates function of all endosomal TLRs (8), no immunostimulatory response was observed (Fig. 3D). Notably, cells expressing the known activating *Unc93b1* D34A mutation identified in the mouse (15) also showed an enhanced TNF- $\alpha$  secretion in response to R848, while TNF- $\alpha$  secretion in response to ODN1668 was reduced (Fig. 3D), consistent with the previously reported inverse effect of D34A on TLR7 and TLR9 signaling (15, 29). Enhanced TLR7 signaling in *Unc93b1*<sup>E92G</sup>-expressing mouse macrophages was confirmed using the ssRNA-analogue poly-uridine (Fig. 3F). Collectively, these findings demonstrate that *Unc93b1*<sup>E92G</sup> confers a gain-of-function, selectively leading to TLR7/8, but not TLR3 or TLR9, hyperactivation.

### The *UNC93B1*<sup>E92G</sup> allele confers an additive gain-of-function

In contrast to the affected members of family B who harbor a dominantly inherited heterozygous *UNC93B1*<sup>R336L</sup> variant, both affected

children of family A carry a homozygous *UNC93B1*<sup>E92G</sup> mutation, raising the question as to the phenotypic effects conferred by *UNC93B1*<sup>E92G</sup>. Given that gain-of-function mutations are usually dominant, we sought to investigate whether the parents of patient 1 and patient 2 (family A), both of whom are healthy heterozygous carriers of the *UNC93B1*<sup>E92G</sup> variant exhibit an intermediate phenotype. To this end, we assessed induced cytokine responses in whole blood following stimulation with the TLR7/TLR8 agonist R848 and the STING agonist ADU-S100, respectively. Stimulation of whole blood with R848 resulted in a strong pro-inflammatory response in both parents compared to healthy controls, with increased production of IL-6, IL-1 $\beta$ , and TNF- $\alpha$  (Fig. 3G). This inflammatory response, however, was not as pronounced as in their affected child (P1; Fig. 3G), despite the fact that he was under treatment with a JAK inhibitor at the time of blood withdrawal and had pro-inflammatory cytokines within normal range at baseline. Notably, like patient 1, both his parents were also less responsive to stimulation with the STING agonist ADU-S100, compared to controls (Fig. 3G), consistent with a negative regulatory role of STING signaling on TLR-dependent autoimmunity (30). Thus, *UNC93B1*<sup>E92G</sup> appears to be semidominant and has a gene dosage effect with large phenotypic effects in homozygous individuals and weaker effects in heterozygous carriers.

### *UNC93B1*<sup>E92G</sup> destabilizes the interaction with TLR7

Recent data on the cryo-EM structures of TLR7 in complex with *UNC93B1*, which assembles as a dimer with a 2:2 stoichiometry, have shown that both TLRs interact with the *UNC93B1* amino-terminal six-helix bundle through their transmembrane and luminal juxta-membrane regions (7). Notably, the overlay of the *UNC93B1*/TLR7 structure in the absence of ligand onto the TLR7 ectodomain structure in the ligand-bound state revealed a steric clash between the two *UNC93B1* molecules because of the tilt angle imposed by the ectodomains (7, 18), suggesting that *UNC93B1* may prevent TLR7 activation by keeping it in an inactive conformation. To explore this further, we examined the consequences of E92G on *UNC93B1* structure. Notably, the E92G mutation lies within the two-turn helix (H1) formed between *UNC93B1* transmembrane domain (TM) 1 and TM2 (residues 91–97) (Fig. 4A). This region was shown to make contact with the two loop regions of the C-terminal LRR-CT motif of the TLR7 ectodomain and to confer rigidity to the orientation of the LRR-CT motif (3, 7). Structural analysis revealed that the E92G mutation on H1 of *UNC93B1* may disrupt potential electrostatic interactions of E92 with nearby residues in the TM5-TM6 loop of *UNC93B1*, such as K273 (7) (Fig. 4A). This is the most extended luminal loop of *UNC93B1*, and disruption of these stabilizing interactions may lead to an increased flexibility of the loop or affect glycosylation of neighboring residues N272 and N251 which are also located on the TM5-TM6 loop (Fig. 4A). Thus, the mutation E92G could potentially lead to destabilization of the *UNC93B1* protein.

The R336L mutation lies within the intracellular helix H3 formed between *UNC93B1* TM6 and TM7 at the interface of the *UNC93B1* dimer which keeps the two TLR7 monomers at a distance and prevents dimerization of the TIR domains (Fig. 4B), the initiating step of TLR7 signaling. Notably, R336 is in close proximity to K333 which was recently shown to undergo ubiquitylation in the context of TLR7 signaling termination (11). Accordingly, K63-linked ubiquitylation of *UNC93B1* along with syntenin-1 recruitment is critical for termination of TLR7 signaling by sorting of *UNC93B1*/TLR7 into intraluminal vesicles (11). As such, *UNC93B1*<sup>R336L</sup> could either interfere with

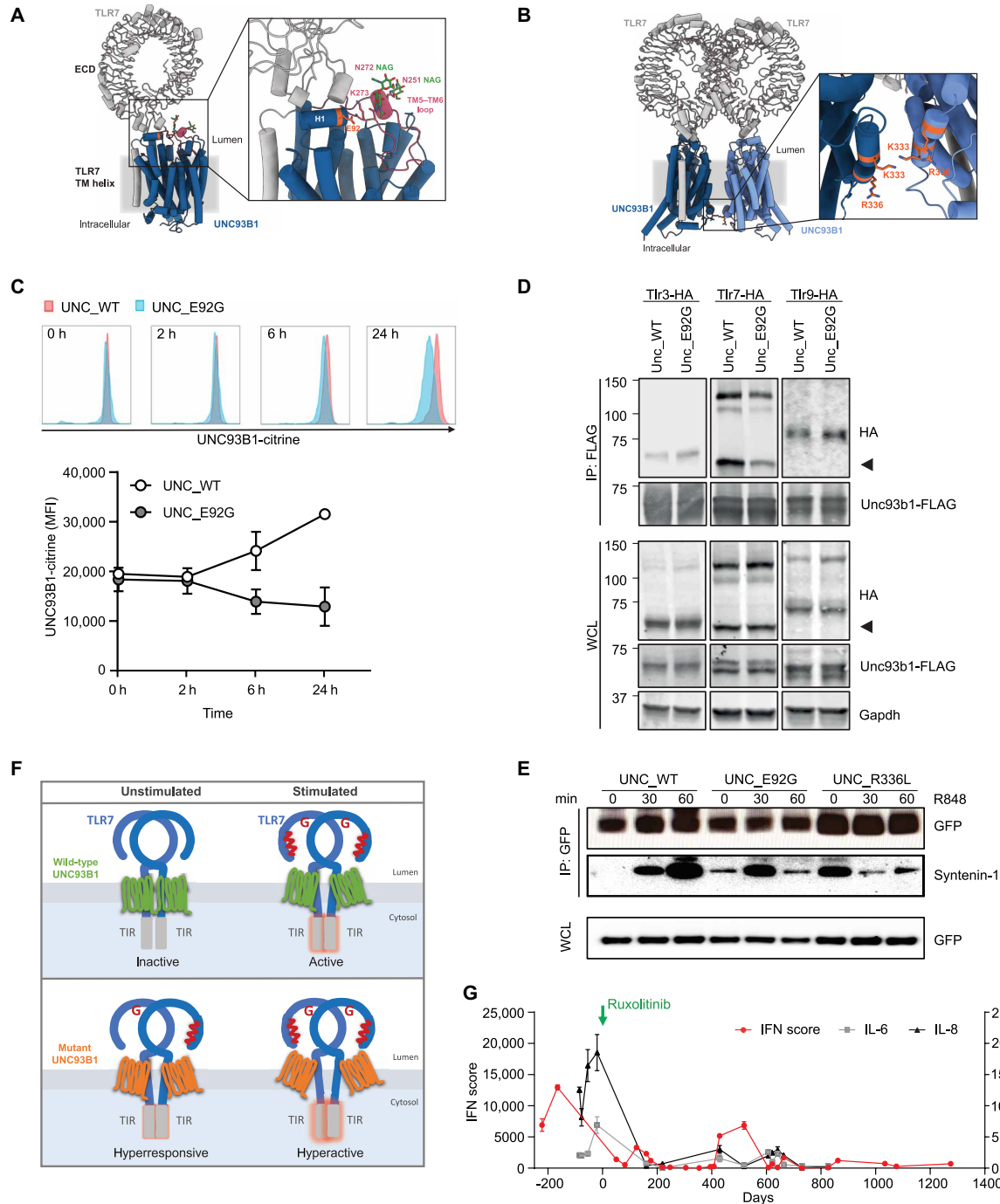


**Fig. 4. UNC93B1 stability, interaction of UNC93B1 with TLR7 and syntenin-1, and effect of ruxolitinib treatment on inflammatory markers.** (A) Structure of TLR7 (grey) bound to UNC93B1 (green) with residue E92 colored in orange (PDB 7CYN). Close-up view of residue E92 on H1 of UNC93B1 and its close proximity to residue K273 on the UNC93B1 TMS-TM6 luminal loop (pink). Glycosylation on residues N272 and N251 is depicted in dark green. (B) Structure of TLR7 (grey) - UNC93B1 (green) dimer. Close-up view of residue R336 and its close proximity to residue K333 on the UNC93B1 TM6-TM7 intracellular loop. UNC93B1 monomers are shown in light and dark green. (C) Stability of wild type (red) and mutant (blue) UNC93B1-citrine expressing HEK293 cells over time, as measured by flow cytometry (upper panel). Quantification of mean fluorescence intensity (MFI) of UNC93B1-citrine expressing cells at indicated time points (mean  $\pm$  SD; n = 3; lower panel). (D) Co-immunoprecipitation of whole cell lysates (WCL) from *Unc93b1*<sup>-/-</sup> RAW264.7 cells reconstituted with Flag-tagged Unc93b1 variants using anti-Flag antibody (IP:Flag), followed by Western blot analysis using anti-HA antibody. Arrow heads indicate active TLR7. Representative data of two independent experiments. (E) Co-immunoprecipitation of whole cell lysates (WCL) from HEK293 cells stably expressing TLR7 and equal levels of citrine-tagged UNC931 variants stimulated with R848 using anti-GFP antibody (IP:GFP), followed by Western blot analysis using anti-syntenin-1 antibody. Representative data of two independent experiments. (F) Model depicting how structural changes imposed by *UNC93B1* mutations could either modify the ligand-binding properties of TLR7 by enhancing binding site accessibility (E92G) or promote signaling initiation by facilitating TIR domain dimerization (R336L), resulting in hyperresponsiveness and hyperactivity of the TLR7 receptor. (G) IFN scores and levels of pro-inflammatory cytokines in blood of patient 1 during treatment with ruxolitinib. Day 0 indicates the start of ruxolitinib treatment.

the inhibitory function of UNC93B1 on TLR7 signaling or impede TLR7 signaling termination, thereby leading to TLR7 hyperactivation.

To further investigate UNC93B1<sup>E92G</sup> protein stability, we measured levels of wild type and mutant UNC93B1-citrine expressed in HEK293 cells after sorting to equal citrine fluorescence intensity ( $t = 0$  h). Compared to wild type UNC93B1, protein levels of the E92G mutant measured at 6 and 24 h were lower (Fig. 4C), indicating reduced protein stability. To assess the impact of E92G on the interaction of Unc93b1 with endosomal Tlrs, we transduced Flag-tagged Unc93b1-reconstituted *Unc93b1*<sup>-/-</sup> RAW264.7 macrophages with HA-tagged Tlr3, Tlr9, and Tlr7, respectively. Despite equal Tlr expression levels, Unc93b1<sup>E92G</sup> interacted less with Tlr7 compared to wild type Unc93b1, as shown by co-immunoprecipitation of Flag-tagged Unc93b1, while the interaction with Tlr3 and Tlr9 was not altered (Fig. 4D). Similarly, Flag-tagged Unc93b1 interacted less with endogenous Tlr7 (fig. S10B). Thus, while Unc93b1<sup>E92G</sup> was able to interact with Tlr7, this interaction was less stable. This is in contrast to the H412R loss-of-function *Unc93b1* mutant, which abolishes interaction with endosomal Tlrs (5) (fig. S10B). Given that ligand binding occurs within the concave side of the horseshoe-shaped ectodomain of TLR7, these findings suggest that a reduced interaction of UNC93B1 with TLR7 due to destabilization of UNC93B1 increases binding site accessibility.

To explore whether disturbed syntenin-1-mediated termination of TLR7 signaling (11) could account for TLR7 hyperactivation observed in our patients, we examined syntenin-1 recruitment to UNC93B1 in response to TLR7 stimulation in HEK293 cells stably expressing TLR7 and equal levels of citrine-tagged UNC93B1 variants. Notably, *UNC93B1*<sup>R336L</sup> lies on the intracellular side where syntenin-1-binding takes place, whereas *UNC93B1*<sup>E92G</sup> localizes on the luminal side of the endosome away from the syntenin-1-binding region (Fig. 4A). While wild type UNC93B1 did not bind to syntenin-1 in the absence of TLR7 stimulation, treatment with R848 led to rapid syntenin-1 recruitment within 30 min which further increased over 60 min, as shown by co-immunoprecipitation of citrine-UNC93B1 (Fig. 4E), confirming this mechanism of TLR7 signaling termination by syntenin-1 also in human cells. Notably, both UNC93B1 mutants showed an association with syntenin-1 already in the absence of R848 stimulation (Fig. 4E), consistent with constitutive activation of TLR7 signaling termination due to TLR7 activation at steady-state in patient cells. Both UNC mutants, however, exhibited distinct dynamics of syntenin-1 recruitment. Syntenin-1-binding to UNC93B1<sup>E92G</sup> was low at baseline, increased at 30 min upon R848 stimulation and subsided to baseline levels after 60 min (Fig. 4E). In contrast, the level of syntenin-1 recruitment to UNC93B1<sup>R336L</sup> at baseline already exceeded that of wild type UNC93B1 at 30 min of R848 stimulation. Following R848 stimulation, syntenin-1-binding to UNC93B1<sup>R336L</sup> did not further increase, but instead was markedly reduced at 30 min with only little increment after 60 min (Fig. 4E). These findings indicate, that chronic TLR7 hyperactivation causes concomitant activation of syntenin-1-dependent signaling termination, which may result in syntenin-1 consumption. Accordingly, TLR7 signaling termination via syntenin-1 per se is not impaired by the *UNC93B1* mutations, although syntenin-1 exhaustion may contribute to TLR7 hyperactivation. Taken together, our findings delineate a pivotal role for UNC93B1 in preventing autoimmunity by restraining uncontrolled TLR7 activation (Fig. 4F).

### Therapeutic response of patient 1 to JAK1/2 inhibition

JAK1/2 inhibitors such as ruxolitinib dampen type I IFN activity by impeding IFN- $\alpha/\beta$  receptor signaling. Consistently, spontaneous type

I IFN signaling in whole blood of patient 1 was efficiently suppressed by ruxolitinib *in vitro* (fig. S11). Given the refractory course of the disease and the very high interferon signature, patient 1 was started on ruxolitinib, which led to a sustained suppression of systemic type I IFN activation with decreased serum levels of IL-8 and IL-6 (Fig. 4G, table S1). This was accompanied by amelioration of transfusion-dependent anemia, panniculitis, and renal disease. However, despite significant clinical improvement, the boy continued to experience flares with systemic inflammation and renal dysfunction (table S1). Several attempts to increase the dose of ruxolitinib to 1 mg/kg to achieve more effective type I IFN inhibition were associated with cytopenia, a known side effect of JAK1/2 inhibitors. Thus, although JAK inhibition is of therapeutic value in patients with TLR7 hyperactivation due to *UNC93B1* mutation, our clinical observations in this patient also reveal a limitation of this approach and highlight the need for more specific TLR7-targeting therapies.

### DISCUSSION

We delineate a monogenic form of SLE caused by mutation in *UNC93B1*, that confers a gain-of-function due to hyperactivation of TLR7 signaling. Engagement of TLR7 by self-RNA derived from endocytosed microbial particles or apoptotic cells initiates downstream signaling pathways resulting in the production of IFN- $\alpha$  and pro-inflammatory cytokines. In SLE, IFN- $\alpha$  drives a self-perpetuating feedback loop that promotes the loss of tolerance and autoimmunity in a non-cell-autonomous manner (26). The clinical and cellular phenotype of the patients resembled that reported for mice carrying the D34A or the PKP530–532 gain-of-function *Unc93b1* mutations, which succumb to TLR7-dependent autoimmunity (11, 15). Our findings in patient cells indicate enhanced activation of ssRNA-sensing TLR7 and TLR8. However, *TLR8* gain-of-function mutations were recently shown to cause increased susceptibility to infections associated with neutropenia and hypogammaglobulinemia (31), whereas a *TLR7* gain-of-function mutation causes SLE (17). In contrast, the SLE patients carrying *UNC93B1* variants had normal neutrophils and exhibited autoimmunity with hypergammaglobulinemia and increased memory-switched B cells, consistent with enhanced B cell hyperresponsiveness caused by TLR7 hyperactivity (table, S1 and S4). Notably, while *TLR8* is predominantly expressed in neutrophils, expression of *TLR7* is restricted to B cells and plasmacytoid dendritic cells in humans (32). This may explain why *TLR8* gain-of-function mutations are associated with neutropenia and infections. Given the pivotal role of B cells and dendritic cells in SLE pathogenesis, this suggests that autoimmunity in our patients is primarily driven by increased TLR7 signaling.

TLR7 harbors two spatially distinct ligand-binding sites within the horseshoe-shaped LRR-CT motif - a first site for guanosine and a second site for short ssRNA (18). Moreover, TLR7 exhibits a synergistic mode of activation in response to its two ligands, whereby successive ligand binding increases binding affinities (18, 33, 34). Similarly, TLR8 was shown to harbor two binding sites for uridine and ssRNA degradation products (28, 35). Notably, host-derived nucleases are not able to fully degrade RNA ligands to prevent self-nucleic acid recognition by TLR7 or TLR8 (28, 36). Given that nucleosides, such as guanosine and uridine, are essential primary metabolites in all living cells, these findings indicate that nucleosides and endogenous degradation products of ssRNA represent natural small TLR7/8 ligands. We propose that engagement of such endogenous ligands dictate TLR7



activity at steady-state and thus fine-tune the general alertness of the TLR7 sensing system under the control by UNC93B1. As binding of both ligands is required for full receptor activation, binding site accessibility critically impacts ligand engagement. Moreover, TLR7 signaling depends on proper dimer assembly, and ligand binding induces a conformational change that reorients the TIR domains to initiate signaling, a process which likely involves some form of dissociation of TLR7 from UNC93B1 (7). Consequently, a loss of structural rigidity that loosens the tight interaction between UNC93B1 and TLR7 could therefore modify the ligand-binding properties of TLR7 by enhancing binding site accessibility (E92G) or promoting signaling initiation by facilitating TIR domain dimerization (R336L). As a result, both UNC93B1 mutations alter the steady-state of TLR7 activation towards a higher responsiveness (Fig. 4F). By demonstrating that E92 is not only important for UNC93B1 stability but also for its interaction with TLR7, we provide further insight into the mechanisms by which the UNC93B1-TLR interaction coordinates TLR signaling. Thus, ligand binding properties of TLRs appear to be dependent on conformational restraints exerted by UNC93B1 on the receptor. Consistent with this notion, an *Unc93b1* mutant that greatly enhances interaction with TLR9 was recently shown to attenuate ligand binding, thereby impeding signaling (37). The inverse logic might apply to the E92G mutant, in which reduced interaction with TLR7 promotes responsiveness. As such, the association strength of UNC93B1 might be a general predictor of TLR responsiveness, whereby increased affinity restricts receptor activity, while reduced affinity liberates activity. The differential effects of E92G on endosomal TLRs may reflect subtype-specific variations in the contact sites with UNC93B1 and the resulting positioning of the ligand-binding sites, suggesting that UNC93B1 controls TLR subtype-specific mechanisms of ligand recognition. In line with TLR subtype-specific functions of UNC93B1, a recently reported glutamic acid insertion (p.Glu49dup) in the UNC93B1 N terminus that selectively impairs the degradative sorting of TLR7, leading to endosomal receptor accumulation, is also associated with human lupus (38).

scRNAseq of PBMCs from patient 1 and patient 3, harboring two different *UNC93B1* mutations, revealed alterations in cell-type composition and dysregulated transcriptional networks that are also observed in patients with complex SLE (Fig. 2, fig. S2). As such, our findings are of particular clinical relevance regarding the management of patients with SLE, patient stratification for clinical trials, and drug development. Unlike JAK inhibitors, which inhibit type I IFN signaling at the level of the IFNAR receptor, TLR7 antagonists target uncontrolled type I IFN activation more upstream at the site where the disease-causing immune signaling is primarily initiated. Given that such TLR7 inhibitory molecules have already been developed and tested preclinically (39, 40), our findings support accelerating further development of TLR7 antagonists for patients with SLE. Interestingly, although *UNC93B1* variants have not previously been implicated in human susceptibility to SLE, a genetic association of an *Unc93b1* variant with cutaneous lupus was recently demonstrated in dogs (41), suggesting that rare variants in human *UNC93B1* may also contribute to the risk for complex SLE.

## MATERIALS AND METHODS

### Study design

In this study, we enrolled 4 patients with early-onset SLE from 2 unrelated families. We collected blood and serum samples for genetic and immunologic investigations. Lymphoblastoid cells and primary fibroblasts derived from skin biopsies were established for functional

analysis. Written informed consent was obtained by all participating members of the families or their legal guardians. The study was approved by the ethics committees of the Medical Faculty, Technische Universität Dresden, and Charité-Universitätsmedizin Berlin and conducted in accordance with the Declaration of Helsinki.

### Whole exome sequencing

Genomic DNA was extracted from blood using Qiamp DNA Blood Mini Kit (Qiagen). For family A, whole exome sequencing was carried out as previously described (42). Constructed exome libraries were subjected to Illumina HiSeq4000/Xten (Illumina) 150 bp paired-end sequencing with an average read depth of 134.5. SOAPnuke was used to remove adapter sequences, low-quality reads and N reads (43). Sequences were mapped to the human reference genome (GRCh37 / UCSC hg19) by Burrows-Wheeler Algorithm (BWA-MEM, version 0.7.10) (44). GATK Haplotype Caller (version 3.3) (45) was used for single nucleotide variants (SNVs) and insertions/deletions (InDels) calling and Ensembl VEP (Variant Effect Predictor) (46) for annotation. For family B, whole exome sequencing was performed following library preparation (SureSelect Human All Exon V6, Agilent) as paired-end next generation sequencing (Illumina, Inc. CA USA). Generated sequence data were analyzed using the Labor Berlin in-house NGS data analysis pipeline (v1.0) and compared to the human reference sequence (hg19). Variant prioritisation was based on allele frequency, variant type, location in the gene, bioinformatic prediction tools, biological function and evidence from literature using VarFish (47) and MutationDistiller (48).

### Sanger sequencing

Genomic DNA flanking the *UNC93B1* (NC\_000011) mutation was amplified by PCR using gene-specific primers (Eurofins MWG Operon; E92\_for- GAATGCCTTCGGTGATTGGAG, E92\_rev-GTTCCTGTTTCCTTCCCCAAATC; R336\_for- GAGCGGAACCTCATTTGTGG, R336\_rev-CGATACCAGTGCAGGCAAAG) and sequenced in both directions using the BigDye Terminator v1.1 Cycle Sequencing Kit (Applied Biosystems) on a 3130xl Genetic Analyzer (Applied Biosystems). Data were analyzed using the Vector NTI Software (Life Technologies).

### Flow Cytometry staining

PBMCs were isolated from EDTA anticoagulated whole blood using Ficoll density centrifugation and stained with the following anti-human antibodies: CD14 (M5E2, BUV395, BD, Cat. No. 740286, 1:50), CD19 (SJ25C1, BV711, BD, Cat. No. 563038, 5:100), CD27 (L128, BV785, BD, Cat. No. 563328, 2:50), CD38 (HIT2, APC-Cy7, BioLegend, Cat. No. 303534, 0.1:50) and IgD (IA6-2, PE-CF594, BioLegend, Cat. No. 348240, 0.1:50). DAPI was added before sample acquisition to allow dead cell exclusion. Gating of plasmablasts was performed as previously described (49). Healthy controls data were from Ferreira-Gomes et al. (50).

### Cell culture

Passage-matched fibroblasts (passages 4–15) were cultured in DMEM complete medium (DMEM high glucose 4.5 g/l supplemented with 2 mM L-Glutamine, 1% antibiotics/ antimycotics, 5% NEAA, 10% FCS). EBV-transformed LCLs were cultured in RPMI-1640 complete medium (RPMI-1640 supplemented with 2 mM L-Glutamine, 1% antibiotics/ antimycotics, 5% NEAA, 10% FCS). For isolation of human PBMCs, whole blood, diluted with PBS, was gently layered over an

equal volume of Biocoll (Sigma-Aldrich) and centrifuged for 30 min at 400 g without brake. The intermediate layer containing PBMCs was removed and added to prewarmed medium.

### Retroviral transduction and fluorescence activated cell sorting

For retroviral transduction of human citrine-tagged UNC93B1 into HEK293 cells, the pR 5' LTR-hUNC93B plasmid was used. The E92G mutation was introduced by site-directed mutagenesis using the QuikChange Lightning Site-Directed Mutagenesis Kit (Agilent). For each viral supernatant to be produced,  $1 \times 10^6$  HEK293T cells were plated in 2 mL complete DMEM. After 24 hours, cells were transfected with retroviral constructs (1  $\mu$ g per well) as well as the retroviral packaging plasmids gag-pol (1  $\mu$ g per well) and VSV-G (1  $\mu$ g per well) using polyethylenimine (Sigma). Cells were incubated at 37°C, 5% CO<sub>2</sub> for 12 hours, prior to medium change. 48 hours upon transfection, the viral supernatant was harvested and added to target cells: HEK293XL-hTLR3-HA, HEK293XL-hTLR7-HA, HEK293XL-hTLR8-HA or HEK293XL-hTLR9-HA cells (Invivogen), seeded to 80% confluence. After 24 h at 37°C, 5% CO<sub>2</sub>, medium was changed to complete DMEM and transduced cells were passaged three times before frozen stocks were prepared. UNC93B1-mCitrine-positive cells were sorted for equal green fluorescence on a FACS Aria cell sorter (BD Biosciences) in a 96 well plate at a density of  $2 \times 10^4$  cells/well in DMEM supplemented with 10% FCS, 2 mM L-glutamine, 1% antibiotics/antimycotics and 1 mg/ml blasticidin.

Haemagglutinin (YPYDVPDYA)-tagged murine TLRs 3, 7 and 9 were expressed in *Unc93b1*<sup>-/-</sup> RAW 264.7 cells using MCSV-Thy1.1 retroviral vectors as previously described (37). For the generation of *Unc93b1*-transgenic RAW264.7 cells, *Unc*\_WT, *Unc*\_H412R and *Unc*\_D34A constructs were generated as previously reported (11) on MCSV-based retroviral vectors with IRES-PuromycinR-T2A-mCherry double selection. *Unc93b1* genes were codon-optimized and contained a 3xFlag C-terminal tag. *Unc*\_E92G construct was generated by site-directed mutagenesis from *Unc*\_WT using Q5 Site Directed Mutagenesis Kit (New England BioLabs) using the following primers: F: CACTACGACGcACATACAGAGAAG and R: CAGGATCAGCTGCATCTG. Viral supernatants were produced by transfecting GP2–293 cells (HEK293-derived packaging cells expressing viral gag and pol proteins) with the *Unc93b1* plasmids (1.7  $\mu$ g per well) along with a VSV-G plasmid (0.8  $\mu$ g per well), pre-incubated with Lipofectamine 3000 transfection reagent (Invitrogen). After overnight incubation at 37°C, the transfected GP2–293 cells were transferred to 32°C for a further 24 hours. Viral supernatants were centrifuged to remove packaging cells before applying to *Unc93b1*<sup>-/-</sup> RAW264.7 target cells, with the addition of polybrene (Sigma-Aldrich). Target cells were centrifuged at 1000 x g for 30 min at 32°C, and further incubated at 32°C overnight before transferring to a 37°C incubator (5% CO<sub>2</sub> maintained throughout). *Unc93b1*-IRES-mCherry-positive RAW264.7 cells were sorted 2 days post-transduction for equal red fluorescence on a FACS Aria II cell sorter (BD Biosciences) and cultured in RPMI supplemented with 10% FCS, L-glutamine, penicillin-streptomycin, sodium pyruvate and HEPES (pH7.2; Invitrogen). *Tlr7* expression in *Unc93b1*-reconstituted RAW264.7 cells was measured by fixation/permeabilization using BD Cytofix/Cytoperm (BD Biosciences), intracellular staining with anti-TLR7 antibody (clone A94B10, MABF2273 Sigma-Aldrich; 1:200) followed by Alexa Fluor 488 goat anti-mouse IgG (A11029, Invitrogen; 1:1000), and data acquisition on a FACS Symphony flow cytometer (BD Biosciences).

### Cytokine analysis

Plasma was collected from blood collected in heparin tubes by centrifugation (2000 rpm) at 4°C for 20 min. Cytokines were measured using the LEGENDplex Human Inflammation Panel 1 (BioLegend) according to the manufacturer's instructions. For experiments using PBMCs or stably transduced HEK293XL cells, cytokines were measured in cell culture supernatants using the LEGENDplex Human Anti-Virus Response Panel (BioLegend) according to the manufacturer's instructions. Data were collected on a FACS flow cytometer (LSRII, Becton Dickinson) and analyzed with the LEGENDplex Data Analysis V8.1 software (BioLegend). For cytokine analysis of whole blood assays, frozen supernatants were thawed on ice and the cytokine concentration was quantified using the CorPlex Human Cytokine Panel 1 10-Plex Array (Quanterix) following the manufacturer's protocol. The samples were acquired on the Quanterix SP-X and raw data was analyzed using the SPX Analysis Application software Version 2.1.1.7737. Cytokine concentration data was loaded into R Version 4.2.2 (R Foundation for Statistical Computing) visualized using the tidyverse package Version 1.3.2 (51). In RAW264.7 cells, TNF- $\alpha$  production was measured by fixation/permeabilization using BD Cytofix/Cytoperm (BD Biosciences) and intracellular staining with APC anti-mouse TNF- $\alpha$  antibody (clone MP6-XT22, 506308 Biolegend; 1:200) followed by acquisition on a CytoFLEX flow cytometer (Beckman Coulter). Flow cytometric data was analysed using FlowJo (Becton Dickinson).

### Immunoprecipitation and Western blot analysis

For Myd88 immunoprecipitation, RAW264.7 cells were incubated with 500 ng/ml R848 at 37°C, 5% CO<sub>2</sub> for 0, 15, 30 or 60 min prior to collection. Cells were collected by scraping in cold PBS and lysed in buffer containing 50 mM Tris-HCl [pH 7.4], 150 mM NaCl, 10% glycerol, 1% NP-40 and supplemented with Complete Protease Inhibitor Cocktail (Roche), PhosSTOP (Roche) and 1 mM PMSF. Cell lysates were incubated for 1 hour on a 4°C rotator and cleared of insoluble material by centrifugation, then incubated with anti-MyD88 antibody (AF3109 R&D Systems; 1  $\mu$ g/sample) overnight, followed by Protein G agarose beads (pre-blocked with 1% BSA) for 2 hours at 4°C the next day. Beads were washed four times in lysis buffer, then precipitated proteins were eluted by heating in SDSxPAGE buffer to 65°C for 15 min.

For Flag immunoprecipitation, RAW264.7 cells were lysed in buffer containing 50 mM Tris-HCl, 150 mM NaCl, 5 mM EDTA, 0.5% NP-40, 1x Complete Protease Inhibitor Cocktail (Roche) and 1 mM PMSF. Cell lysates were incubated for 1 hour on a 4°C rotator and cleared of insoluble material by centrifugation, then incubated with M2 anti-Flag matrix (Sigma) (pre-blocked with 1% BSA) for 2 hours on a 4°C rotator. Beads were washed four times in lysis buffer, then precipitated proteins were competitively eluted with 150 ng/ $\mu$ l 3xFlag-peptide (Sigma) in lysis buffer for 30 min at room temperature. Eluted proteins were denatured in SDSxPAGE buffer for 1 hour at room-temperature. Proteins were separated by SDS-PAGE (Bio-Rad TGX precast gels) and transferred to Immobilon PVDF membranes (Millipore) in a Trans-Blot Turbo transfer system (Bio-Rad). Membranes were probed with antibodies against MyD88 (AF3109 R&D Systems; 1:200), IRAK2 (#4367 CST; 1:1000), Flag (clone M2, F1804, Sigma-Aldrich; 1:1000), HA (3F10, Roche), and GAPDH (GA1R, MA5–15738 Invitrogen; 1:2000). Blots were developed using the ChemiDoc MP system (Bio-Rad).

For GFP immunoprecipitation, HEK293 cells were lysed in NP-40 buffer (50 mM Tris [pH 7.4], 150 mM NaCl, 0.5% NP-40, 5 mM EDTA)

supplemented with 40 mM N-ethylmaleimide (Sigma), 1x Complete Protease Inhibitor Cocktail, and 1x PhosSTOP phosphatase inhibitors (Roche). After incubation at 4°C for 1 hour, lysates were cleared of insoluble material by centrifugation. For immunoprecipitations, lysates were incubated with ChromoTek GFP-Trap Magnetic Agarose (proteintech) for 2 hours at 4°C, and washed twice in PBS containing 0.5% NP-40. Precipitated proteins were eluted and denatured in 2x SDS loading buffer at room temperature for 1 hour. LCLs were lysed in RIPA buffer (50 mM Tris-HCl [pH 7.4], 150 mM NaCl, 1 mM EDTA, 1% Triton X-100, 1 mM sodium orthovanadate, 20 mM sodium fluoride) supplemented with 1x Complete Protease Inhibitor Cocktail, 1x PhosSTOP phosphatase inhibitors (Roche) and DNase I (Qiagen). Protein concentration was determined using a BCA Kit (Thermo Scientific). Lysates and GFP-immunoprecipitated proteins were resolved in a 4–12% NuPAGE Bis-Tris gel and blotted onto a nitrocellulose membrane (BA83, Sigma-Aldrich). Membranes were blocked in 5% dry milk and probed with the following antibodies diluted 1:1000 in 5% BSA: rabbit-anti-TLR7 (CST #5632), rabbit-anti-Syntenin (CST #27964), rabbit-anti-GFP (CST #2956) and mouse-anti- $\beta$ -actin (Sigma-Aldrich #A5316). Immunoreactive signals were detected by chemiluminescence using Lumi-Light PLUS (Roche).

### Cell stimulation

Cells were stimulated as indicated with poly(I:C) HMW (tlrl-pic, Invivogen); R848 (resiquimod, tlrl-r848, Invivogen); Pam2CSK4 (tlrl-pm2s-1, Invivogen); ODN2006 (tlrl-2006, Invivogen), ODN1668 (5'-TCCATGACGTTCCCTGATGCT-3', all phosphorothioate linkages, synthesized by Integrated DNA Technologies), LPS-EB Ultrapure (tlrl-3pelps, Invivogen), polyU<sub>19</sub>mer (all phosphorothioate linkages, Integrated DNA Technologies), ssRNA40 (ssRNA40 5'-GCCCCUGUGUGACUC-3', Eurofins MWG Operation). If not otherwise indicated, ssRNA40 and ODN2006 were complexed in a 1:1 ratio with poly-L-arginine (Sigma-Aldrich). Unless otherwise specified, cells were stimulated for 24 hours at 37°C and 5% CO<sub>2</sub>. RAW264.7 macrophages were stimulated for 6 hours at 37°C and 5% CO<sub>2</sub>, with the addition of BD GolgiPlug at 1:1000 dilution after 30 min of stimulation.

### Whole blood assay

For analysis of the effect of ruxolitinib on type I IFN signaling *in vitro*, heparin blood was distributed in 24 well plates at 1 ml per well. Plates were incubated on a shaker incubator at 300 rpm and 37°C. For type I IFN activation, blood was incubated with 1  $\mu$ g/ml poly(I:C) (HMW, Invivogen) for 5 hours and then either treated with 1  $\mu$ M and 2  $\mu$ M ruxolitinib (MedChemExpress) or left untreated for additional 10 hours. After erythrocyte lysis, samples were frozen at -80°C and subsequently used for RNA extraction. For analysis of induced cytokine responses in family A, hirudin blood was diluted with cell culture media in a ratio of 1:3 and activated with 100 ng/ml R848 (InvivoGen) or 10  $\mu$ g/ml ADU-S100 (MedChemExpress) for 6 hours at 37°C and centrifuged at 230 g for 5 min at room temperature. For analysis of specific TLR responses, whole blood was diluted 1:1 with RPMI cell culture media and stimulated for 24 hours with 5  $\mu$ g/ml R837 (InvivoGen), 100 ng/ml TL8-506 (InvivoGen) or 1  $\mu$ M ODN2216 (InvivoGen).

### Quantitative real-time RT-PCR

Total RNA was extracted from PBMCs or from lysed whole blood using the ReliaPrep RNA Cell Miniprep System (Promega) followed by

DNase I digestion. RNA was reverse transcribed using the GoScript Reverse Transcription System (Promega). Gene expression was determined by quantitative real-time RT-PCR using the Taqman Universal PCR Master Mix (Applied Biosystems) on an ABI7300 and normalized to glyceraldehyde-3-phosphate dehydrogenase (for-GAAGGTGAAGTTCGGAGTC, rev-GAAGATGGTGATGGGATTTC, and FAM-CAAGCTTCCCGTTCTCAGCC-TAMRA) and hypoxanthine phosphoribosyltransferase 1 (Hs02800695\_m1; Thermo Fisher) expression. For calibration, a calibrator cDNA was included in each assay. Target genes were analyzed using predesigned TaqMan probes (Thermo Fisher) for *IFI27* (Hs01086373\_g1), *IFI44* (Hs00951349\_m1), *IFI44L* (Hs00915292\_m1), *IFIT1* (Hs01675197\_m1), *ISG15* (Hs01921425\_s1), *RSAD2* (Hs01057264\_m1), and *SIGLEC1* (Hs00988063\_m1). The IFN score was calculated as previously described (42).

### Protein Structure Modeling

Illustration of the complex TLR7-UNC93B1 (PDB 7CYN) was prepared using UCSF ChimeraX (52).

### Statistical analysis

Statistical analysis was carried out in GraphPad PRISM6 as indicated. For normally distributed variables, parametric tests were used, including t-test for comparison of two groups and one-way ANOVA with post hoc tests, as indicated, for comparison of three or more groups. For variables with non-normal distribution, non-parametric tests were employed. For comparison of two groups, Mann-Whitney U test was used for independent variables and Wilcoxon signed-rank test was used for dependent variables. For comparison of three or more group variables, Kruskal-Wallis test was utilized. Values of  $P < 0.05$  were considered statistically significant. Data are represented as means  $\pm$  SD.

### Supplementary Materials

#### This PDF file includes:

Figs. S1 to S11  
Tables S1 to S4  
References (53–55, 57–61)

#### Other Supplementary Material for this manuscript includes the following:

Data File S1 and S2  
MDAR Reproducibility Checklist

### REFERENCES AND NOTES

1. N. A. Lind, V. E. Rael, K. Pestal, B. Liu, G. M. Barton, Regulation of the nucleic acid-sensing Toll-like receptors. *Nat. Rev. Immunol.* **22**, 224–235 (2022).
2. K. Pelka, T. Shibata, K. Miyake, E. Latz, Nucleic acid-sensing TLRs and autoimmunity: Novel insights from structural and cell biology. *Immunol. Rev.* **269**, 60–75 (2016).
3. I. Botos, D. M. Segal, D. R. Davies, The structural biology of toll-like receptors. *Structure* **19**, 447–459 (2011).
4. Y.-M. Kim, M. M. Brinkmann, M.-E. Paquet, H. L. Ploegh, UNC93B1 delivers nucleotide-sensing toll-like receptors to endolysosomes. *Nature* **452**, 234–238 (2008).
5. M. M. Brinkmann, E. Spooner, K. Hoebe, B. Beutler, H. L. Ploegh, Y.-M. Kim, The interaction between the ER membrane protein UNC93B and TLR3, 7, and 9 is crucial for TLR signaling. *J. Cell Biol.* **177**, 265–275 (2007).
6. K. Pelka, D. Bertheloot, E. Reimer, K. Phulphagar, S. V. Schmidt, A. Christ, R. Stahl, N. Watson, K. Miyake, N. Hacohen, A. Haas, M. M. Brinkmann, A. Marshak-Rothstein, F. Meissner, E. Latz, The Chaperone UNC93B1 Regulates Toll-like Receptor Stability Independently of Endosomal TLR Transport. *Immunity* **48**, 911–922.e7 (2018).



7. H. Ishida, J. Asami, Z. Zhang, T. Nishizawa, H. Shigematsu, U. Ohto, T. Shimizu, Cryo-EM structures of Toll-like receptors in complex with UNC93B1. *Nat. Struct. Mol. Biol.* **28**, 173–180 (2021).
8. K. Tabeta, K. Hoebe, E. M. Janssen, X. Du, P. Georgel, K. Crozat, S. Mudd, N. Mann, S. Sovath, J. Goode, L. Shamel, A. A. Herskovits, D. A. Portnoy, M. Cooke, L. M. Tarantino, T. Wiltshire, B. E. Steinberg, S. Grinstein, B. Beutler, The Unc93b1 mutation 3d disrupts exogenous antigen presentation and signaling via Toll-like receptors 3, 7 and 9. *Nat. Immunol.* **7**, 156–164 (2006).
9. A. Casrouge, S.-Y. Zhang, C. Eidenschenck, E. Jouanguy, A. Puel, K. Yang, A. Alcais, C. Picard, N. Mahfoufi, N. Nicolas, L. Lorenzo, S. Plancoulaine, B. Sénéchal, F. Geissmann, K. Tabeta, K. Hoebe, X. Du, R. L. Miller, B. Héron, C. Mignot, T. B. de Villemeur, P. Lebon, O. Dulac, F. Rozenberg, B. Beutler, M. Tardieu, L. Abel, J.-L. Casanova, Herpes simplex virus encephalitis in human UNC-93B deficiency. *Science* **314**, 308–312 (2006).
10. J.-W. Huh, T. Shibata, M. Hwang, E.-H. Kwon, M. S. Jang, R. Fukui, A. Kanno, D.-J. Jung, M. H. Jang, K. Miyake, Y.-M. Kim, UNC93B1 is essential for the plasma membrane localization and signaling of Toll-like receptor 5. *Proc. Natl. Acad. Sci. U.S.A.* **111**, 7072–7077 (2014).
11. O. Majer, B. Liu, L. S. M. Kreuk, N. Krogan, G. M. Barton, UNC93B1 recruits syntenin-1 to dampen TLR7 signalling and prevent autoimmunity. *Nature* **575**, 366–370 (2019).
12. S. R. Christensen, J. Shupe, K. Nickerson, M. Kashgarian, R. A. Flavell, M. J. Shlomchik, Toll-like receptor 7 and TLR9 dictate autoantibody specificity and have opposing inflammatory and regulatory roles in a murine model of lupus. *Immunity* **25**, 417–428 (2006).
13. P. Pisitkun, J. A. Deane, M. J. Difilippantonio, T. Tarasenko, A. B. Satterthwaite, S. Bolland, Autoreactive B cell responses to RNA-related antigens due to TLR7 gene duplication. *Science* **312**, 1669–1672 (2006).
14. S. Subramanian, K. Tus, Q.-Z. Li, A. Wang, X.-H. Tian, J. Zhou, C. Liang, G. Bartov, L. D. McDaniel, X. J. Zhou, R. A. Schultz, E. K. Wakeland, A Tlr7 translocation accelerates systemic autoimmunity in murine lupus. *Proc. Natl. Acad. Sci. U.S.A.* **103**, 9970–9975 (2006).
15. R. Fukui, S.-I. Saitoh, A. Kanno, M. Onji, T. Shibata, A. Ito, M. Onji, M. Matsumoto, S. Akira, N. Yoshida, K. Miyake, Unc93B1 restricts systemic lethal inflammation by orchestrating Toll-like receptor 7 and 9 trafficking. *Immunity* **35**, 69–81 (2011).
16. S. A. Jenks, K. S. Cashman, E. Zumaquero, U. M. Marigorta, A. V. Patel, X. Wang, D. Tomar, M. C. Woodruff, Z. Simon, R. Bugrovsky, E. L. Blalock, C. D. Scharer, C. M. Tipton, C. Wei, S. S. Lim, M. Petri, T. B. Niewold, J. H. Anolik, G. Gibson, F. E.-H. Lee, J. M. Boss, F. E. Lund, I. Sanz, Distinct effector b cells induced by unregulated toll-like receptor 7 contribute to pathogenic responses in systemic lupus erythematosus. *Immunity* **49**, 725–739.e6 (2018).
17. G. J. Brown, P. F. Cañete, H. Wang, A. Medhavy, J. Bones, J. A. Roco, Y. He, Y. Qin, J. Cappello, J. I. Ellyard, K. Bassett, Q. Shen, G. Burgio, Y. Zhang, C. Turnbull, X. Meng, P. Wu, E. Cho, L. A. Miosge, T. D. Andrews, M. A. Field, D. Tvorogov, A. F. Lopez, J. J. Babon, C. A. López, A. González-Murillo, D. C. Garulo, V. Pascual, T. Levy, E. J. Mallack, D. G. Calame, T. Lotze, J. R. Lupski, H. Ding, T. R. Ullah, G. D. Walters, M. E. Koina, M. C. Cook, N. Shen, C. de Lucas Collantes, B. Corry, M. P. Gantier, V. Athanasopoulos, C. G. Vinuesa, TLR7 gain-of-function genetic variation causes human lupus. *Nature* **605**, 349–356 (2022).
18. Z. Zhang, U. Ohto, T. Shibata, E. Krayukhina, M. Taoka, Y. Yamauchi, H. Tanji, T. Isobe, S. Uchiyama, K. Miyake, T. Shimizu, Structural analysis reveals that toll-like receptor 7 is a dual receptor for guanosine and single-stranded RNA. *Immunity* **45**, 737–748 (2016).
19. D. Nehar-Belaid, S. Hong, R. Marches, G. Chen, M. Bolisetty, J. Baisch, L. Walters, M. Punaro, R. J. Rossi, C.-H. Chung, R. P. Huynh, P. Singh, W. F. Flynn, J.-A. Tabanor-Gayle, N. Kuchipudi, A. Mejias, M. A. Collet, A. L. Lucido, K. Palucka, P. Robson, S. Lakshminarayanan, O. Ramilo, T. Wright, V. Pascual, J. F. Banchereau, Mapping systemic lupus erythematosus heterogeneity at the single-cell level. *Nat. Immunol.* **21**, 1094–1106 (2020).
20. C. Guiducci, M. Gong, Z. Xu, M. Gill, D. Chaussabel, T. Meeker, J. H. Chan, T. Wright, M. Punaro, S. Bolland, V. Soumelis, J. Banchereau, R. L. Coffman, V. Pascual, F. J. Barrat, TLR recognition of self nucleic acids hampers glucocorticoid activity in lupus. *Nature* **465**, 937–941 (2010).
21. R. K. Perez, M. G. Gordon, M. Subramaniam, M. C. Kim, G. C. Hartoularos, S. Targ, Y. Sun, A. Ogorodnikov, R. Bueno, A. Lu, M. Thompson, N. Rappoport, A. Dahl, C. M. Lanata, M. Matloubian, L. Maliskova, S. S. Kwek, T. Li, M. Slyper, J. Waldman, D. Dionne, O. Rozenblatt-Rosen, L. Fong, M. Dall'Era, B. Balliu, A. Regev, J. Yazdany, L. A. Criswell, N. Zaitlen, C. J. Ye, Single-cell RNA-seq reveals cell type-specific molecular and genetic associations to lupus. *Science* **376**, eabf1970 (2022).
22. A. M. Jacobi, M. Odendahl, K. Reiter, A. Bruns, G. R. Burmester, A. Radbruch, G. Valet, P. E. Lipsky, T. Dörner, Correlation between circulating CD27high plasma cells and disease activity in patients with systemic lupus erythematosus. *Arthritis Rheum.* **48**, 1332–1342 (2003).
23. F. Heil, H. Hemmi, H. Hochrein, F. Ampenberger, C. Kirschning, S. Akira, G. Lipford, H. Wagner, S. Bauer, Species-specific recognition of single-stranded RNA via toll-like receptor 7 and 8. *Science* **303**, 1526–1529 (2004).
24. A. Kuznik, M. Bencina, U. Svajger, M. Jeras, B. Rozman, R. Jerala, Mechanism of endosomal TLR inhibition by antimalarial drugs and imidazoquinolines. *J. Immunol.* **186**, 4794–4804 (2011).
25. I. B. Bekerjian-Ding, M. Wagner, V. Hornung, T. Giese, M. Schnurr, S. Endres, G. Hartmann, Plasmacytoid dendritic cells control TLR7 sensitivity of naive B cells via type I IFN. *J. Immunol.* **174**, 4043–4050 (2005).
26. A. Marshak-Rothstein, Toll-like receptors in systemic autoimmune disease. *Nat. Rev. Immunol.* **6**, 823–835 (2006).
27. F. P. Siegal, N. Kadowaki, M. Shodell, P. A. Fitzgerald-Bocarsly, K. Shah, S. Ho, S. Antonenko, Y. J. Liu, The nature of the principal type 1 interferon-producing cells in human blood. *Science* **284**, 1835–1837 (1999).
28. W. Greulich, M. Wagner, M. M. Gaidt, C. Stafford, Y. Cheng, A. Linder, T. Carell, V. Hornung, TLR8 Is a Sensor of RNase T2 Degradation Products. *Cell* **179**, 1264–1275.e13 (2019).
29. R. Fukui, S. Saitoh, F. Matsumoto, H. Kozuka-Hata, M. Oyama, K. Tabeta, B. Beutler, K. Miyake, Unc93B1 biases Toll-like receptor responses to nucleic acid in dendritic cells toward DNA- but against RNA-sensing. *J. Exp. Med.* **206**, 1339–1350 (2009).
30. S. Sharma, A. M. Campbell, J. Chan, S. A. Schattgen, G. M. Orlowski, R. Nayyar, A. H. Huyler, K. Nardal, K. Mohan, L. J. Berg, M. J. Shlomchik, A. Marshak-Rothstein, K. A. Fitzgerald, Suppression of systemic autoimmunity by the innate immune adaptor STING. *Proc. Natl. Acad. Sci. U.S.A.* **112**, E710–E717 (2015).
31. J. Aluri, A. Bach, S. Kaviyani, L. Chiquetto Paracatu, M. Kitcharoensakul, M. A. Walkiewicz, C. D. Putnam, M. Shinawi, N. Saucier, E. M. Rizzi, M. T. Harmon, M. P. Keppel, M. Ritter, M. Similuk, E. Kulm, M. Joyce, A. A. de Jesus, R. Goldbach-Mansky, Y.-S. Lee, M. Cella, P. L. Kendall, M. C. Dinauer, J. J. Bednarski, C. Bemrich-Stolz, S. W. Canna, S. M. Abraham, M. M. Demczko, J. Powell, S. M. Jones, A. M. Scurlock, S. S. De Ravin, J. J. Bleesing, J. A. Connelly, V. K. Rao, L. G. Schuettelpelz, M. A. Cooper, Immunodeficiency and bone marrow failure with mosaic and germline TLR8 gain of function. *Blood* **137**, 2450–2462 (2021).
32. V. Hornung, S. Rothenfusser, S. Britsch, A. Krug, B. Jahrsdörfer, T. Giese, S. Endres, G. Hartmann, Quantitative expression of toll-like receptor 1-10 mRNA in cellular subsets of human peripheral blood mononuclear cells and sensitivity to CpG oligodeoxynucleotides. *J. Immunol.* **168**, 4531–4537 (2002).
33. Z. Zhang, U. Ohto, T. Shibata, M. Taoka, Y. Yamauchi, R. Sato, N. M. Shukla, S. A. David, T. Isobe, K. Miyake, T. Shimizu, Structural Analyses of toll-like receptor 7 reveal detailed RNA sequence specificity and recognition mechanism of agonistic ligands. *Cell Rep.* **25**, 3371–3381.e5 (2018).
34. T. Shibata, U. Ohto, S. Nomura, K. Kibata, Y. Motoi, Y. Zhang, Y. Murakami, R. Fukui, T. Ishimoto, S. Sano, T. Ito, T. Shimizu, K. Miyake, Guanosine and its modified derivatives are endogenous ligands for TLR7. *Int. Immunol.* **28**, 211–222 (2016).
35. H. Tanji, U. Ohto, T. Shibata, M. Taoka, Y. Yamauchi, T. Isobe, K. Miyake, T. Shimizu, Toll-like receptor 8 senses degradation products of single-stranded RNA. *Nat. Struct. Mol. Biol.* **22**, 109–115 (2015).
36. T. Ostendorf, T. Zillinger, K. Andryka, T. M. Schlee-Guimaraes, S. Schmitz, S. Marx, K. Bayrak, R. Linke, S. Salgert, J. Wegner, T. Grasser, S. Bauersachs, L. Soltesz, M. P. Hübner, M. Nastaly, C. Coch, M. Kettwig, I. Roehl, M. Henneke, A. Hoerauf, W. Barchet, J. Gärtner, M. Schlee, G. Hartmann, E. Bartok, Immune sensing of synthetic, bacterial, and protozoan RNA by toll-like receptor 8 requires coordinated processing by RNase T2 and RNase 5. *Immunity* **52**, 591–605.e6 (2020).
37. O. Majer, B. Liu, B. J. Woo, L. S. M. Kreuk, E. Van Dis, G. M. Barton, Release from UNC93B1 reinforces the compartmentalized activation of select TLRs. *Nature* **575**, 371–374 (2019).
38. H. Mishra, C. Schlack-Leigers, E. L. Lim, O. Thieck, T. Magg, J. Raedler, C. Wolf, C. Klein, H. Ewers, M. A. Lee-Kirsch, D. Meierhofer, F. Hauck, O. Majer, Endosome dysfunction leads to gain-of-function TLR7 and human lupus. *bioRxiv*. 2023, <https://www.biorxiv.org/content/10.1101/2023.04.03.535356v1.full>
39. S. Hawtin, C. André, G. Collignon-Zipfel, S. Appenzeller, B. Bannert, L. Baumgartner, D. Beck, C. Betschart, T. Boulay, H. I. Brunner, M. Ceci, J. Deane, R. Feifel, E. Ferrero, D. Kyburz, F. Lafossas, P. Loetscher, C. Merz-Stoekle, P. Michellys, B. Nuesslein-Hildesheim, F. Raulf, J. S. Rush, G. Ruzzante, T. Stein, S. Zaharevitz, G. Wiczorek, R. Siegel, P. Gergely, T. Shisha, T. Junt, Preclinical characterization of the Toll-like receptor 7/8 antagonist MHV370 for lupus therapy. *Cell. Rep. Med.* **4**, 101036 (2023).
40. T. Shisha, M. G. Posch, J. Lehmann, R. Feifel, T. Junt, S. Hawtin, J. Schuemann, A. Avrameas, R. Danekula, P. Misiolek, R. Siegel, P. Gergely, First-in-Human Study of the Safety, Pharmacokinetics, and Pharmacodynamics of MHV370, a Dual Inhibitor of Toll-Like Receptors 7 and 8, in Healthy Adults. *Eur. J. Drug Metab. Pharmacokinet.* **48**, 553–566 (2023).
41. T. Leeb, F. Leuthard, V. Jagannathan, S. Kiener, A. Letko, P. Roosje, M. M. Welle, K. L. Gailbreath, A. Cannon, M. Linek, F. Banovic, T. Olivry, S. D. White, K. Batchler, D. Bannasch, K. M. Minor, J. R. Mickelson, M. K. Hytönen, H. Lohi, E. A. Mauldin, M. L. Casal, A Missense Variant Affecting the C-Terminal Tail of UNC93B1 in Dogs with Exfoliative Cutaneous Lupus Erythematosus (ECL). *Genes (Basel)* **11**, 159 (2020).
42. C. Wolf, N. Brück, S. Koss, C. Griep, M. Kirschfink, K. Palm-Beden, M. Fang, N. Röber, S. Winkler, R. Berner, E. Latz, C. Günther, M. A. Lee-Kirsch, Janus kinase inhibition in complement component 1 deficiency. *J. Allergy Clin. Immunol.* **146**, 1439–1442.e5 (2020).
43. Y. Chen, Y. Chen, C. Shi, Z. Huang, Y. Zhang, S. Li, Y. Li, J. Ye, C. Yu, Z. Li, X. Zhang, J. Wang, H. Yang, L. Fang, Q. Chen, SOAPnuke: A MapReduce acceleration-supported software for integrated quality control and preprocessing of high-throughput sequencing data. *Gigascience* **7**, 1–6 (2018).



44. H. Li, R. Durbin, Fast and accurate long-read alignment with Burrows-Wheeler transform. *Bioinformatics* **26**, 589–595 (2010).
45. A. McKenna, M. Hanna, E. Banks, A. Sivachenko, K. Cibulskis, A. Kernytsky, K. Garimella, D. Altshuler, S. Gabriel, M. Daly, M. A. DePristo, The Genome Analysis Toolkit: A MapReduce framework for analyzing next-generation DNA sequencing data. *Genome Res.* **20**, 1297–1303 (2010).
46. W. McLaren, L. Gil, S. E. Hunt, H. S. Riat, G. R. S. Ritchie, A. Thormann, P. Flicek, F. Cunningham, The Ensembl variant effect predictor. *Genome Biol.* **17**, 122 (2016).
47. M. Holtgrewe, O. Stolpe, M. Nieminen, S. Mundlos, A. Knaus, U. Kornak, D. Seelow, L. Segebrecht, M. Spielmann, B. Fischer-Zirnsak, F. Boschmann, U. Scholl, N. Ehmke, D. Beule, VarFish: Comprehensive DNA variant analysis for diagnostics and research. *Nucleic Acids Res.* **48**, W162–W169 (2020).
48. D. Hombach, M. Schuelke, E. Knierim, N. Ehmke, J. M. Schwarz, B. Fischer-Zirnsak, D. Seelow, MutationDistiller: User-driven identification of pathogenic DNA variants. *Nucleic Acids Res.* **47**, W114–W120 (2019).
49. F. Szelinski, A. L. Stefanski, E. Schrezenmeier, H. Rincon-Arevalo, A. Wiedemann, K. Reiter, J. Ritter, M. Lettau, V. D. Dang, S. Fuchs, A. P. Frei, T. Alexander, A. C. Lino, T. Dörner, Plasmablast-like Phenotype Among Antigen-Experienced CXCR5–CD19lowB Cells in Systemic Lupus Erythematosus. *Arthritis Rheumatol.* **74**, 1556–1568 (2022).
50. M. Ferreira-Gomes, A. Kruglov, P. Durek, F. Heinrich, C. Tizian, G. A. Heinz, A. Pascual-Reguant, W. Du, R. Mothes, C. Fan, S. Frischbutcher, K. Habenicht, L. Budzinski, J. Ninnemann, P. K. Jani, G. M. Guerra, K. Lehmann, M. Matz, L. Ostendorf, L. Heiberger, H.-D. Chang, S. Bauherr, M. Maurer, G. Schönrich, M. Raftery, T. Kallinich, M. A. Mall, S. Angermair, S. Treskatsch, T. Dörner, V. M. Corman, A. Diefenbach, H.-D. Volk, S. Elezkurtaj, T. H. Winkler, J. Dong, A. E. Hauser, H. Radbruch, M. Witkowski, F. Melchers, A. Radbruch, M.-F. Mashreghi, SARS-CoV-2 in severe COVID-19 induces a TGF- $\beta$ -dominated chronic immune response that does not target itself. *Nat. Commun.* **12**, 1961 (2021).
51. H. Wickham, M. Averick, J. Bryan, W. Chang, L. D. McGowan, R. François, G. Grolemond, A. Hayes, L. Henry, J. Hester, M. Kuhn, T. L. Pedersen, E. Miller, S. M. Bache, K. Müller, J. Ooms, D. Robinson, D. P. Seidel, V. Spinu, K. Takahashi, D. Vaughan, C. Wilke, K. Woo, H. Yutani, Welcome to the Tidyverse. *J. Open Source Softw.* **4**, 1686 (2019).
52. T. D. Goddard, C. C. Huang, E. C. Meng, E. F. Pettersen, G. S. Couch, J. H. Morris, T. E. Ferrin, UCSF ChimeraX: Meeting modern challenges in visualization and analysis. *Protein Sci.* **27**, 14–25 (2018).
53. M. Witkowski, C. Tizian, M. Ferreira-Gomes, D. Niemeyer, T. C. Jones, F. Heinrich, S. Frischbutcher, S. Angermair, T. Hohnstein, I. Mattioli, P. Nawrath, S. McEwen, S. Zocche, E. Viviano, G. A. Heinz, M. Maurer, U. Kölsch, R. L. Chua, T. Aschman, C. Meisel, J. Radke, B. Sawitzki, J. Roehmel, K. Allers, V. Moos, T. Schneider, L. Hanitsch, M. A. Mall, C. Conrad, H. Radbruch, C. U. Duerr, J. A. Trapani, E. Marcenaro, T. Kallinich, V. M. Corman, F. Kurth, L. E. Sander, C. Drosten, S. Treskatsch, P. Durek, A. Kruglov, A. Radbruch, M.-F. Mashreghi, A. Diefenbach, Untimely TGF $\beta$  responses in COVID-19 limit antiviral functions of NK cells. *Nature* **600**, 295–301 (2021).
54. Y. Huang, D. J. McCarthy, O. Stegle, Vireo: Bayesian demultiplexing of pooled single-cell RNA-seq data without genotype reference. *Genome Biol.* **20**, 273 (2019).
55. C. S. McGinnis, L. M. Murrow, Z. J. Gartner, DoubletFinder: Doublet detection in single-cell RNA sequencing data using artificial nearest neighbors. *Cell Syst.* **8**, 329–337.e4 (2019).
56. F. A. Wolf, P. Angerer, F. J. Theis, SCANPY: Large-scale single-cell gene expression data analysis. *Genome Biol.* **19**, 15 (2018).
57. Y. Xu, S. J. Baumgart, C. M. Stegmann, S. Hayat, MACA: Marker-based automatic cell-type annotation for single-cell expression data. *Bioinformatics* **38**, 1756–1760 (2022).
58. Y. Hao, S. Hao, E. Andersen-Nissen, W. M. Mauck, S. Zheng, A. Butler, M. J. Lee, A. J. Wilk, C. Darby, M. Zager, P. Hoffman, M. Stoeckius, E. Papalexi, E. P. Mimitou, J. Jain, A. Srivastava, T. Stuart, L. M. Fleming, B. Yeung, A. J. Rogers, J. M. McElrath, C. A. Blish, R. Gottardo, P. Smibert, R. Satija, Integrated analysis of multimodal single-cell data. *Cell* **184**, 3573–3587.e29 (2021).
59. E. Y. Chen, C. M. Tan, Y. Kou, Q. Duan, Z. Wang, G. V. Meirelles, N. R. Clark, A. Ma'ayan, Enrichr: Interactive and collaborative HTML5 gene list enrichment analysis tool. *BMC Bioinformatics* **14**, 128 (2013).
60. A. Butler, P. Hoffman, P. Smibert, E. Papalexi, R. Satija, Integrating single-cell transcriptomic data across different conditions, technologies, and species. *Nat. Biotechnol.* **36**, 411–420 (2018).
61. M. Ringer, K. Costenbader, D. Daikh, R. Brinks, M. Mosca, R. Ramsey-Goldman, J. S. Smolen, D. Wofsy, D. T. Boumpas, D. L. Kamen, D. Jayne, R. Cervera, N. Costedoat-Chalumeau, B. Diamond, D. D. Gladman, B. Hahn, F. Hiepe, S. Jacobsen, D. Khanna, K. Lerström, E. Massarotti, J. McCune, G. Ruiz-Irastorza, J. Sanchez-Guerrero, M. Schneider, M. Urowitz, G. Bertsias, B. F. Hoyer, N. Leuchten, C. Tani, S. K. Tedeschi, Z. Touma, G. Schmajuk, B. Anic, F. Assan, T. M. Chan, A. E. Clarke, M. K. Crow, L. Czirják, A. Doria, W. Graninger, B. Halda-Kiss, S. Hasni, P. M. Izmirly, M. Jung, G. Kumánovics, X. Mariette, I. Padjen, J. M. Pego-Reigosa, J. Romero-Diaz, I. Rúa-Figueroa Fernández, R. Seror, G. H. Stummvoll, Y. Tanaka, M. G. Tektonidou, C. Vasconcelos, E. M. Vital, D. J. Wallace, S. Yavuz, P. L. Meroni, M. J. Fritzler, R. Naden, T. Dörner, S. R. Johnson, 2019 European League Against Rheumatism/American College of Rheumatology classification criteria for systemic lupus erythematosus. *Ann. Rheum. Dis.* **78**, 1151–1159 (2019).

**Acknowledgments:** We thank the patients and their family for participation in the study. We thank Anne Gompf, Rainer Stahl, and Markus Utzt for technical assistance, Shen-Ying Zhang and Jean-Laurent Casanova for UNC93B1-deficient patient cells, and Tobias Straub and the Bioinformatic Core Facility for providing compute infrastructure. We acknowledge the assistance of the flow cytometry and the imaging facilities of the Center for Molecular and Cellular Bioengineering and the Medical Theoretical Centre, TU Dresden, the flow cytometry and sequencing facilities of the Deutsches Rheuma-Forschungszentrum, Berlin, as well as the LAFUGA sequencing facility of the Gene Center LMU, Munich. **Funding:** The study was supported by German Research Foundation (DFG) grants KFO249 160548243 (MLK), CRC237 369799452/B21 (MLK, JK), CRC237 369799452/A11 (MLK, EL), CRC237 369799452/A06 (CW), KI 1956/2-1 (BK) and the Emmy Noether Program 458004906 (COM), the German Federal Ministry of Education and Research grants 01GM2206C (MLK) CONAN and TREAT (MFM), an Else-Kröner-Fresenius-Stiftung starting grant 2019\_A70 (JK), the Leibniz Association, Leibniz Collaborative Excellence, TargArt (TK, MFM) and ImpACT (FMF), the Berlin Institute of Health with the state of Berlin and the European Regional Development Fund (ERDF 2014–2021, EFRE 1.8/11, Deutsches Rheuma-Forschungszentrum) (MFM), a Berlin Institute of Health Fellowship (TK), a Berlin Institute of Health Clinical Scientist Program Fellowship (CCG), and the Max Planck Society (ELL, OM). **Author contributions:** Conceptualization: CW, MLK; Methodology: CW, ELL, MoM, PW, AS, EB, MFM, SVS, JK, OM, MLK; Investigation: CW, ELL, MoM, BK, AO, ELV, SK, SM, KM, KE, GD, BB, DTS, KS, TN, CCG, PW, KM, TD, AS, FS, GG, MM, MB, CCO, EB, TK, MFM, SVS, EL, JK, OM, MLK; Visualization: CW, EL, MoM, COM, JK, OM; Funding acquisition: CW, ELL, BK, EL, COM, MFM, TK, CCG, JK, OM, MLK; Project administration: MLK; Supervision: CW, JK, OM, MLK; Writing – original draft: CW, MLK; Writing – review & editing: CW, JK, OM, MLK. **Competing interests:** EL is co-founder and advisor of IFM Therapeutics, Odyssey Therapeutics and Beren Therapeutics. All other authors declare that they have no competing interests. **Data and materials availability:** scRNA-seq data reported in this study have been deposited in the Single Cell Portal for interactive viewing and download (accession number SCP2151) as well as GEO (accession number GSE250223). Jupyter notebooks and scripts used for the analysis of scRNA-seq data are available on GitHub ([https://github.com/KlughammerLab/UNC93B1\\_scrRNAseq](https://github.com/KlughammerLab/UNC93B1_scrRNAseq)) and Zenodo (<https://zenodo.org/doi/10.5281/zenodo.10395384>). Tabulated data underlying the figures are provided in Data file S1 and uncropped Western blots in Data file S2. All other data needed to support the conclusions of the paper are available in the main text or the supplementary materials.

Submitted 30 May 2023  
Accepted 22 December 2023  
Published 11 January 2024  
10.1126/sciimmunol.adi9769

## Abstract

**One-sentence summary:** UNC93B1 prevents human lupus by restraining uncontrolled TLR7 activation.